Acta Pharmaceutica Sinica B 2025;15(3):1359−1382

Chinese Pharmaceutical Association
Institute of Materia Medica, Chinese Academy of Medical Sciences

Acta Pharmaceutica Sinica B

www.elsevier.com/locate/apsb
www.sciencedirect.com

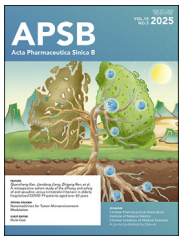

ORIGINAL ARTICLE

Targeting farnesoid X receptor as aging intervention therapy

Lijun Zhang[a], Jing Yu[a], Xiaoyan Gao[a], Yingxuan Yan[a], Xinyi Wang[a], Hang Shi[a], Minglv Fang[a], Ying Liu[a], Young-Bum Kim[b], Huanhu Zhu[c], Xiaojun Wu[d,*], Cheng Huang[a,*], Shengjie Fan[a,*]

[a]*School of Pharmacy, Shanghai University of Traditional Chinese Medicine, Shanghai 201203, China*
[b]*Division of Endocrinology, Diabetes, and Metabolism, Beth Israel Deaconess Medical Center and Harvard Medical School, Boston, MA 02115, USA*
[c]*School of Life Science and Technology, ShanghaiTech University, Shanghai 201210, China*
[d]*Institute of Chinese Materia Medica, Shanghai University of Traditional Chinese Medicine, Shanghai 201203, China*

Received 22 August 2024; received in revised form 21 October 2024; accepted 14 November 2024

KEY WORDS

Obeticholic acid;
Farnesoid X receptor;
Lifespan;
Healthspan;
Aging;
Detoxification;
Pregnane X receptor;
Longevity

Abstract Environmental toxicants have been linked to aging and age-related diseases. The emerging evidence has shown that the enhancement of detoxification gene expression is a common transcriptome marker of long-lived mice, *Drosophila melanogaster*, and *Caenorhabditis elegans*. Meanwhile, the resistance to toxicants was increased in long-lived animals. Here, we show that farnesoid X receptor (FXR) agonist obeticholic acid (OCA), a marketed drug for the treatment of cholestasis, may extend the lifespan and healthspan both in *C. elegans* and chemical-induced early senescent mice. Furthermore, OCA increased the resistance of worms to toxicants and activated the expression of detoxification genes in both mice and *C. elegans*. The longevity effects of OCA were attenuated in $Fxr^{-/-}$ mice and *Fxr* homologous *nhr-8* and *daf-12* mutant *C. elegans*. In addition, metabolome analysis revealed that OCA increased the endogenous agonist levels of the pregnane X receptor (PXR), a major nuclear receptor for detoxification regulation, in the liver of mice. Together, our findings suggest that OCA has the potential to lengthen lifespan and healthspan by activating nuclear receptor-mediated detoxification functions, thus, targeting FXR may offer to promote longevity.

*Corresponding authors.
E-mail addresses: xiaojunwu@shutcm.edu.cn (Xiaojun Wu), chuang@shutcm.edu.cn (Cheng Huang), shengjiefan@shutcm.edu.cn (Shengjie Fan).
Peer review under the responsibility of Chinese Pharmaceutical Association and Institute of Materia Medica, Chinese Academy of Medical Sciences.

https://doi.org/10.1016/j.apsb.2025.01.006

1. Introduction

Environmental factors are one of the major reasons impacting the lifespan of humans. The xenobiotics such as residue of patricides in foods and water, environmental and estrogen contamination, drugs and their metabolites, and the endobiotics, such as bacterial endotoxin, amine, ketone, and metabolites of glucose, lipids, and amino acids, may result in damage of cells and tissues, consequently accelerating senescence[1-4]. The xeno/endobiotic detoxification is emerging as a target for aging-extension. Inhibition of the insulin/insulin-like growth factor-1 signaling (IIS) pathway may extend the lifespan in *C. elegans*, *Drosophila*, and mammals, accompanying the increased resistance to various stressors, such as oxidative and xenobiotic stress[5,6]. In long-lived *C. elegans*, DAF-16, the ortholog of Forkhead Box O (FOXO), plays essential roles in the aging-retarding and detoxification under the suppression of IIS signaling[7-9]. Similarly, in long-lived flies, the functions of dFOXO are the same as in *C. elegans*[10]. In dietary and methionine-restriction long-lived mice, the resistance to hepatotoxins acetaminophen, thioacetamide, and bleomycin is significantly increased[11-14].

Recently, increasing evidence shows that the expression of detoxification genes is enhanced in long-lived animals[15]. The increase in the expression of detoxification genes was identified in several long-lived mice. For example, in genetic long-lived growth hormone-releasing hormone receptor knockout Little mice and growth hormone deficient Ames dwarf mice, the livers' detoxification genes were increased and showed more resistance to liver toxins[16,17]. Similar observation was found in the pituitary abnormal Snell dwarf mice and growth hormone receptor knockout mice[18,19]. A recent study has found that the transcription levels of detoxification enzymes, cytochrome P450s (*Cyps*) and glutathione-*S*-transferases (*Gsts*), were increased in the livers of mice with lifespan-extending interventions. Enhancing detoxification functions is a common transcriptome marker of all long-lived mice[20], suggesting that the upregulation of detoxification enzymes may be a potential anti-aging therapy.

The detoxification genes were mainly expressed in the liver and transcriptionally regulated by nuclear hormone receptors (NHRs), including pregnane X receptor (PXR), constitutive androstane receptor (CAR), farnesoid X receptor (FXR), liver X receptor, vitamin D receptor in mammals. There is growing evidence that age-related changes in the liver are a risk factor for the pathogenesis of age-related diseases[21]. FXR is a primary bile acid receptor with the highest expression levels in the liver and transcriptionally regulates a group of genes for glucose, lipid, and bile acid homeostasis. FXR agonist OCA has been marketed for the treatment of primary biliary cholangitis[22] and is a potential drug for nonalcoholic steatohepatitis[23]. Interestingly, FXR protein levels are elevated in the livers of the long-lived Little mice (*Ghrhr(lit/lit)*), which is associated with the expression of xenobiotic genes *Abcb1a*, *Fmo3*, and *Gsta2*, as well as the increase of the resistance to a variety of xenobiotics[16,24,25]. Although it is unknown whether the activation of FXR may delay the aging process, recent studies have shown that FXR is associated with aging-related disorders. FXR and G protein-coupled receptor 5 dual agonist INT-767 may reverse age-related kidney disease and estrogen-dependent bone loss in mice[26,27]. Lack of FXR would result in energy metabolism disorders and liver damage in aged mice[28,29]. In contrast, activation of FXR may improve skeletal muscle loss in aged mice[30]. These data suggest that FXR directly transcriptionally targets xenobiotic genes, and FXR may be a critical regulator of longevity.

In *C. elegans*, NHR-8 and DAF-12 are the homolog of mammal nuclear receptors, transcriptionally regulating the expression of detoxification enzymes and ATP binding cassette (ABC) transporters to excrete toxins. NHR-8 is required for *C. elegans* longevity by DR[31,32]. In germline cell deficient long-lived *C. elegans*, deletion of DAF-12 reduced the lifespan and healthspan[33,34]. DAF-12 agonist also extends the lifespan of *glp*-1/*daf-36* mutants[35]. In contrast, the gain function of DAF-12 mutants showed more health and a longer lifespan[36], suggesting that Both NHR-8 and DAF-12 are required for the longevity of *C. elegans*. Here, we show that the FXR agonist OCA may extend lifespan and healthspan in *C. elegans* and mice through the activation of FXR signaling.

2. Materials and methods

2.1. Materials

OCA (CAS No. 459789-99-2) was obtained from TOPHARMAN (Shanghai, China) with purity ≥99.2%. OCA stock solution was prepared using dimethyl sulfoxide (DMSO 100%) to 100 mmol/L. Work solutions were diluted in *Escherichia coli* OP50, resulting in the final concentrations at 5, 10, 20, 50, and 100 μmol/L. Doxorubicin (Dox) (CAS No. 25316-40-9) was purchased from Shanghai Yuanye BioTech (Shanghai, China) with purity >93%. D-Galactose (D-gal) (CAS No. 59-23-4) with purity ≥98% was purchased from Sigma, USA.

2.2. Nematode strains and maintenance

All worms were cultured at 20 °C on solid nematode growth medium (NGM) plate pre-seeded with standard food resource *E. coli* OP50[37]. The *C. elegans* strains used in this study included N2 Bristol strain (wild type), *daf-12* (*rh61rh411*), *nhr-8* (*tm1800*), *daf-2* (*e1370*), *daf-16* (*mu86*), DAF-16:: GFP (*muIs 186*), *eat-2* (*ad1116*), *sir-2.1* (*ok434*), *aak-2* (*ok524*), *nhr8*$^{-/-}$, *daf-16*::GFP, *daf-12*$^{-/-}$, *daf-16*::GFP, *let-363* (*ok3018*), *raga-1* (*ok386*), *fat-2* (*wa17*), *fat-3* (*ok1126*), *fat-5* (*tm420*), *fat-6* (*tm331*), and *fat-7* (*wa36*). These strains were all gained from Prof. Huanhu Zhu's lab as gifts. The synchronized worm population was obtained by sodium hypochlorite treatment[38].

2.3. Lifespan assay

Lifespan analysis was carried out at 20 °C as mentioned previously with modifications[39]. When the synchronized nematodes

grew to the L4 stage (Day 0 for lifespan assays), the nematodes were transferred to the NGM culture plate inoculated with chemical-containing *E. coli* OP50, and refreshed plate for 5 consecutive days until reproduction ceased, then worms were removed from the petri dish every other day and recorded the number of dead worms until the last worm died. Animals that did not move in response to a light mechanical touch to the head with a picker were rated as dead. Animals exhibited bagging, exploring, or crawling off the plates were not counted. All statistical analyses were performed by Prism 7 (GraphPad) and SPSS Statistics 21 (IBM). *P* values were calculated by the log-rank (Kaplan−Meier) method. All lifespans contained three biological replicates for each experiment.

2.4. Locomotion and pharyngeal pumping rate assays

Synchronized worms were cultured for lifespan analysis, and locomotion and pumping rates were recorded as previous methods[40]. The head bending and pharyngeal pumping rate assay were carried out on Days 3, 5, 7, 9, 11, 13, and 15 to determine the number of head twisting and pharynx swallowing of ten nematodes within 1 min. At least 10 worms were in one test, and the experiment was repeated three times. The motion assays were carried out on Days 9, 11, 13, and 15, and motion was classified into 3 groups, Motion A: nematodes moved freely, Motion B: nematodes moved slowly after stimulation, Motion C: nematodes only moved head and tail after prodding. ($n = 50$ nematodes in each group each time).

2.5. Bacterial growth and avoidance assays

Liquid bacterial growth was performed in transparent, flat-bottomed 96-well plates to determine the food quality of *C. elegans* as previously described[41]. Briefly, *E. coli* strain OP50 was previously grown overnight in Lennox Broth (LB) media and maintained at 37 °C with constant shaking for about 14−16 h. Then 200 μL of *E. coli* OP50 containing OCA at the desired concentrations as required (0, 5, 10, 20, and 50 μmol/L). The absorbance of each well was determined at OD 595 nm using a Microplate Reader (BioTek Instruments, Synergy, HT). At least 3 independent individuals were carried out in each experiment.

To assess the avoidance of compounds, DMSO and OCA at 5, 10, 20, and 50 μmol/L were mixed with OP50 and then plated on the NGM plate. Then, a drop of M9 containing 50 worms was added in the middle of the plates. Every hour, the number of worms at each spot was counted. At least 3 independent individuals were carried out in each experiment.

2.6. Fertility assay

Ten synchronized wild-type L4 nematodes were transferred to NGM dish with or without OCA for one worm per dish, and the number of eggs laid was counted. The nematode was transferred to a fresh dish every 24 h until egg production ceased. All plates were continued to be cultured in the 20 °C incubator to record the number of eggs hatched. The experiment was repeated three times.

2.7. DAF-16::GFP nuclear localization assay

Synchronized L1 larvae were inoculated on the NGM plates pretreated with the lawn of *E. coli* OP50 containing 10 μmol/L OCA. The worms were cultured to the L4 stage, anesthetized with 20% sodium azide (NaN_3), and picked on the microscopic glass slide with 2% agarose pad. Confocal microscopy was performed using a Leica SP-8 instrument (Germany). Count at least 10 worms to analyze the nucleus localization, and the experiments were repeated three times.

2.8. Stress resistance assay

For the oxidative stress resistance assay, the wild-type worms were cultured with 10 μmol/L OCA for 5 days according to lifespan assay and then transferred the day 6 adult worms to a new petri dish containing hydrogen peroxide (H_2O_2, final concentration: 8 mmol/L). The dead worms were recorded every hour until all worms died.

For heat stress resistance, the nematodes were cultured for 5 days and then transferred to a 35 °C incubator, the dead worms were recorded every hour until all worms died. When worms were straightforward, and had no response to a picker, it was recorded as dead. These assays were repeated 3 times with 60 individuals per assay.

2.9. Transcriptomic profiling and computational analysis

For each sample, approximately 10,000 synchronized young adult nematodes were collected, which were treated with or without 10 μmol/L OCA. The nematodes were washed with M9 buffer about 5 times to remove bacteria, and collected samples were snap-frozen in liquid nitrogen and stored at −80 °C. RNA extraction of all samples was performed at the same time. Total RNA was isolated using a TRIzol total RNA extraction kit (TIANGEN). High-quality RNA with an $A_{260/280}$ ratio of 1.8−2.2 was used for library construction and sequencing. The sequencing was performed using the Illumine NovaSeq 6000 sequencing platform (Paired-end 150) to generate raw reads. Raw paired-end fastq reads were filtered by TrimGloreto discard the adapters and low-quality bases *via* calling the Cutadapt tool[42]. The clean reads were obtained using HISAT2[43], followed by reference genome-guided transcriptome assembly and gene expression quantification using String Tie[44]. Differentially expressed genes (DEG) were identified by DEseq 2 (for samples with replications)[45] or edgeR (for samples without replication) with a cut-off value of log2 |fold change| > 1 and *P*-adjust <0.05. The clusterProfiler[46] was used to perform functional enrichment analysis for the annotated significant DEGs, the potential genes in identified modules based on gene ontology (GO) and KEGG pathway categories. Terms with *P* value < 0.05 were considered significant. Gene set enrichment analysis (GSEA) was performed by the function in package clusterProfiler with a gene list sorted by log2 fold-change.

2.10. RNA interference (RNAi)

RNAi analysis of *cyp35a3*, *cyp35b3*, *gst-4*, *gst-10*, *ugt-44*, and *pgp-3* was performed as described previously[47]. Briefly, RNAi bacteria were grown at 37 °C in LB liquid medium overnight with 50 μg/mL ampicillin and then seeded onto the NGM plate containing 50 μg/mL ampicillin and 1 mg/mL isopropylthiogalactoside (IPTG), cultured overnight. L1 stage N2 worms were transferred onto the plate with RNAi bacteria lawn until the L4 stage, and RNAi lifespan assay used L4 stage worms. Nematodes were subsequently transferred to another fresh RNAi dish every day until the post-reproductive stage and then transferred every other day until the death of the last one. Count deaths daily or

every other day. The RNAi lifespan assays were performed as mentioned in lifespan assays, the nematodes were maintained at 20 °C.

2.11. *nhr-8 and daf-12 hybrid with DAF-16::GFP nuclear localization assays*

Crossed synchronized L1 larvae were inoculated to NGM plates with 10 μmol/L OCA cultured to L4 larvae, anaesthetized with 20% sodium azide (NaN_3), and picked on the microscopic glass slide with 2% agarose pad. Confocal microscopy was performed using a Leica SP-8 instrument (Germany). Count 10 worms in which the nucleus localized, and the experiment repeated three times.

2.12. *Toxicity assay*

Exogenous toxic substances methylmercury chloride (MeHgCl), paraquat (PQ), colchicine (CC), and chloroquine (CQ) were used to test the detoxification effect of OCA. The nematodes were treated with or without OCA for 6 days according to lifespan assays, and then picked into 96-well microplate containing 2 μmol/L MeHgCl, 200 mmol/L PQ, 4 mmol/L CC, and 4 mmol/L CQ with 0, 0.625, 1.25, 2.5, 5 and 10 μmol/L OCA, respectively, then picked 8−10 worms into per well using picker, and totally 48−60 individuals were used as one experiment. All experiments were repeated 3 times and the data were expressed as mean ± standard error of mean (SEM).

2.13. *Confocal microscopy and analysis of mitochondrial integrity in C. elegans*

Worms *myo-3p::TOMM-20::mKate2::HA* (*foxSi16*) were mounted on the indicated days on 2% agarose pad and anesthetized using 20% sodium azide (NaN_3). Mounted nematodes were imaged by a microscope with an RFP filter (Zeiss, Germany). At least 10 worms were imaged per group. Body muscle mitochondria RFP fluorescence intensity was qualified by ImageJ.

2.14. *Animal experiments*

2.14.1. *Dox-induced accelerated aging mice*

All animals' procedures for this study were approved by the Shanghai University of Traditional Chinese Medicine (Approval Number: PZSHUTCM211018017). All mice were housed at constant temperature (22−23 °C), and on a 12 h light and 12 h dark cycle with food and water *ad libitum*. All animals were housed in their new environment for 1 week before starting the experiment. Dox was used to induce senescence in mice. Male C57BL/6J mice (8 weeks) were intraperitoneally injected with Dox at 5 mg/kg body weight. The control group mice were injected with an equivalent volume of saline. For lifespan, the mice were continued to be administrated with Dox (5 mg/kg at a dose of 0.1 mL/10 g body weight) twice weekly and OCA (5 mg/kg/day) until all mice died. For healthspan experiments, the mice received Dox (5 mg/kg three times per week) intraperitoneally for 2 weeks and OCA (5 mg/kg/day) through gavage for 4 weeks. At the end of the healthspan experiments, the mice performed the pole test and balance beam. The mice were euthanized, and the blood and tissues were collected for further analysis.

FXR null knockout mice for lifespan experiments were obtained from Prof. Furong Qiu of Shuguang Hospital, Shanghai University of Traditional Chinese Medicine. Twenty-four male and female mice were divided into two groups according to age; the Dox group and OCA group (n = 12 in each group). Dox-induced senescence and OCA treatment were performed as indicated above. At the same time, wild-type mice were employed as controls. After administration of Dox for 8 weeks, the pole test and balance beam were tested as above.

2.14.2. *D-gal-induced premature mice*

Thirty male C57BL/6 mice (6-week-old) were purchased from the SLAC Laboratory (Shanghai, China). Animals were divided into 3 groups; control group, D-gal (300 mg/kg), and D-gal-induced mice treated with OCA (D-gal: 300 mg/kg body weight, OCA: 2 mg/kg body weight) with 10 mice in each group. After eight weeks of continuous treatment with D-gal and OCA, the behavioral tests were performed. At the end of the animal experiment, mice were fasted overnight and anesthetized using 20% urethane, and cardiac blood and tissues were collected for further analysis.

2.14.3. *Senescence accelerated mouse P8 (SAMP8)*

Twenty SAMP8 mice (12-week-old) and 10 senescence-accelerated mouse resistant 1 (SAMR1) mice were purchased from Beijing HFK Bioscience, China. SAMP8 mice were divided into two groups randomly according to their body weight. OCA was mixed into the food, at a 4.5 mg/1000 g diet. After acclimating for 1 week, mice were fed with the diet with OCA and the chow diet. Then the behavior of them was tested, and body weight and food intake were measured once a week.

2.14.4. *Behavioral test*

2.14.4.1. Pole tests. The pole test was performed to evaluate motor function. Briefly, each mouse was placed on the small ball (diameter 2.5 cm), the head was up-forward, and recorded the time of turning on the ball and climbing down from the pole (diameter 1 cm, height 52 cm), respectively. Before the test, mice were trained 3 times, and then tested 2 times, the data were averaged by two tests.

2.14.4.2. Balance beam test. Balance beam test was performed to measure the coordination and balance, a cylindrical wooden stick (diameter is 1 cm and 50 cm in length) was placed on the cage using medical tape. The mice were placed on one side of the stick, and the time that the mouse reached the other side of the wooden stick was recorded. Each mouse was pre-trained 3 times and then tested 2 times. When the mouse walked from the stick for more than 30 s, the passing time was recorded as 30 s.

2.14.4.3. Rotarod test. The rotarod test is assayed to measure motor coordination and balance[48]. Briefly, the mouse was trained 3 times before the test, and the speed (rpm) was slowly increased from 5 to 40 at a uniform speed. The time and frequency of fall from the rotarod rod were recorded.

2.14.4.4. Open field test. The Open field test serves as a useful method to assess locomotor activity and emotional responses[49]. Simply, the mice were individually put into an open field black tank (50 cm × 50 cm × 50 cm). Each mouse was put in the center of the field gently. The behavior was recorded for 15 min. The time spent travelling in the center area of the open field and the

total travelling distance were analyzed by a video-tracking system (Noldus Information Technology™, Leesburg, VA, USA).

2.14.4.5. Elevated plus maze test. The elevated plus maze test was employed to evaluate anxiety-related behavior as described previously[50]. The maze consisted of two open arms (30 cm × 5 cm), two closed arms (30 cm × 5 cm × 15 cm), and a central area (5 cm × 5 cm), all of those were elevated 60 cm above the floor. Each mouse was placed into the center area facing an open arm to begin a test and explored 15 min freely. The time and entries spent in both open and closed arms were recorded respectively.

2.14.4.6. Y-maze test. The Y-maze test was used to assess spatial memory ability[51]. It consists of a start arm, a secondary arm, and a novel arm (blocked during the training trial, and opened during the test). The angle between each arm is 120°. In the training trial, the mouse freely explored the two arms (start arm and secondary arm) for 10 min. After 2 h, we performed the test in which each mouse was put in the maze at the start arm and allowed to explore all arms for 10 min. The time and entries spent in the novel arm were recorded.

2.14.4.7. Noval object recognition test. The novel object recognition test is employed to assess the working memory[52]. The test was carried out in a 50 cm × 50 cm × 50 cm white box. During the training phases, two identical objects "A" were put in the chamber, and the mouse was allowed to explore the objects for 5 min. When the head of the mouse is facing the object and the nose is within 2 cm of the object, it is considered to be exploration. After 2 h, one of the subjects "A" was replaced with "B" and performed as above. After 24 h, another "A" was replaced with "C". The exploratory time and frequency of the two objects (novel and familiar) were recorded. At the experimental interval of each behavior test, cleaning and wiping with 75% alcohol to eliminate the effect of odor between mice.

2.14.5. Histological analysis

On the last day of the behavioral test, mice were fasted overnight and anesthetized using 20% urethane, and the cardiac blood, the liver, heart, and brain tissues were collected. For histological analysis, the liver, heart, and brain tissues were fixed in 4% formalin solution, embedded in paraffin, cut at 5 μm and stained with hematoxylin-eosin (HE), Sirius red, Masson trichrome and TUNEL staining according to standard procedures. The morphology was observed with a microscope (Zeiss, Germany). Image J was used to quantify the images.

2.15. Cell viability assay

L02 Cell viability was determined by Cell Counting Kit-8 (CCK8) (TargetMol, Cat: C0005). L02 cells were plated into 96-well plates at a density of 100,000 cells per well overnight, and then treated with OCA for 24 h and added different toxins (PQ, MeHgCl, CQ, CC, and Dox) for 48 h. After incubation, 10% volume CCK-8 was added and cells were incubated for 0.5−4 h. The OD values were measured at 450 nm by the multi-mode reader (Bio Tek Instruments Inc., USA). The cell viability was calculated as Eq. (1):

$$\text{Cell viability}\ (\%) = (\text{OD values of OCA group} - \text{OD values of blank group}) / (\text{OD values of toxin group} - \text{OD values of blank group}) \quad (1)$$

2.16. Untargeted identification of the metabolite profile

2.16.1. LC−MS analysis

An accurately 20 mg weighed liver sample was transferred to a 1.5 mL Eppendorf tube. In each tube, two small steel balls and 600 μL of methanol−water (*v*:*v* = 4:1, containing 4 μg/mL of L-2-chlorophenyl alanine) were added. Samples were stored at −40 °C for 2 min and then grinded at 65 HZ for 2 min, and the whole sample was extracted by ultrasonic for 10 min in an ice-water bath, stored at −40 °C for 2 h. The extract was centrifuged at 13,000 rpm (Eppendorf, 5424, Hamburg, Germany), 4 °C for 10 min. After absorbing 150 μL supernatant, the samples were filtered by 0.22 μm membrane and then were collected into LC vials, and stored at −80 °C until LC−MS/MS analysis. The quality control samples were prepared by mixing the extracts of all samples in the same volume.

ACQUITY UPLC I-Class system (Waters Co., Milford, USA) and QE HF mass spectrometer (Thermo Fisher Scientific) with an ACQUITY UPLC HSS T3 (100 mm × 2.1 mm, 1.8 μm) column were used to analyze metabolite profiles in both ESI positive and negative modes. The mobile phase consisted of (A) water and (B) acetonitrile, both containing 0.1% formic acid. The flow rate was 0.35 mL/min and the column temperature was 45 °C. The elution program was as follows: 0.01−2 min, 95% A; 4 min, 70% A; 8 min, 50% A; 10 min, 20% A; 14−15 min, 0% A; 15.1 min, 95% A; 16 min, 95% A.

Data acquisition was performed in full scan mode (*m*/*z* 70 to 1000), and the parameters of the mass spectrometer were as follows: Resolution (full scan), 60,000; Resolution (HCD MS/MS scans), 15,000; Spray voltage, 3800 V (+) and 3000 V (−); Sheath and aux gas flow rate, 35 and 8 Arb; and Capillary temperature, 320 °C.

Quality controls were injected at regular intervals throughout the analytical run to provide a set of data from which repeatability could be assayed.

The original LC−MS data were processed by the software Progenesis QI V2.3 (Nonlinear, Dynamics, Newcastle, UK) for baseline filtering, peak identification, integral, retention time correction, peak alignment, and normalization. Main parameters of 5 ppm precursor mass-to-charge ratio (*m*/*z*), secondary fragments, and isotopic distribution using The Human Metabolome Database (HMDB), Lipidmaps (V2.3), Metlin, EMDN, PMDB, and self-built database to do qualitative analysis. The extracted data were then further processed by removing any peaks with a missing value (ion intensity = 0) in more than 50% of groups, by replacing the zero value with half of the minimum value, and by screening according to the qualitative results of the compound. Compounds with resulting scores below 36 (out of 60) points were also deemed to be inaccurate and removed. A data matrix was combined from the positive and negative ion data.

The matrix was imported in R to carry out Principal Component Analysis (PCA) to observe the overall distribution among the samples and the stability of the whole analysis process. Orthogonal Partial Least-Squares-Discriminant Analysis (OPLS-DA) and Partial Least-Squares-Discriminant Analysis (PLS-DA) were utilized to distinguish the metabolites that differ between groups. To prevent overfitting, 7-fold cross-validation and 200 Response Permutation Testing (RPT) were used to evaluate the quality of the model.

Variable Importance of Projection (VIP) values obtained from the OPLS-DA model were used to rank the overall contribution of

each variable to group discrimination. A two-tailed Student's *t*-test was further used to verify whether the metabolites of difference between groups were significant. Differential metabolites were selected with VIP values greater than 1.0 and p-values less than 0.05.

2.16.2. GC−MS analysis

Methoxyl amine hydrochloride in pyridine (15 mg/mL, 80 μL) was added into the glass vial, vortex shake for 2 min, and then shake the vial at 37 °C for 60 min in an incubator for oxime reaction. Then 50 μL of BSTFA derivatization reagent, 20 μL of hexane, 10 μL of 10 internal standards, vortex shake for 2 min, and then reacted at 70 °C for 60 min. The samples were placed at room temperature for 30 min until GC−MS analysis.

The derivative samples were analyzed on an Agilent 7890B gas chromatography system consisting of an Agilent 5799B MSD system (Agilent Technologies Inc., CA, USA). A DB-5MS (30 m × 0.25 mm × 0.25 μm, Agilent J & W Scientific, Folsom, CA, USA) was used to separate the derivatives. The carrier gas was Helium (>99.999%) at a flow rate of 1 mL/min and an inlet temperature of 260 °C. The injection volume was 1 μL with no split injection and the solvent delay time was set to 6.2 min.

The initial temperature of the column oven was 60 °C for 0.5 min; programmed ramp-up to 125 °C at a rate of 8 °C/min; to 210 °C at a rate of 8 °C/min; to 270 °C at a rate of 15 °C/min; to 305 °C at a rate of 20 °C/min and finally held at 305 °C for 5 min.

The parameters of the mass spectrometer are as follows: Electron bombardment ion source (EI), ion source temperature, 230 °C, quadrupole temperature, 150 °C, electron energy, 70 eV. Mass spectrometric data was acquired in a full-scan mode (*m/z* 50−500).

Quality controls were injected at regular intervals throughout the analytical run to provide a set of data from which repeatability could be assayed. The obtained GC/MS raw data in .D format were transferred to .abf format *via* the software Analysis Base File Converter for quick retrieval of data. Then, data were imported into the software MS-DIAL, which performs peak detection, peak identification, MS2Dec deconvolution, characterization, peak alignment, wave filtering, and missing value interpolation. Metabolite characterization is based on the LUG database. A data matrix was derived. The three−dimensional matrix includes sample information, the name of the peak of each substance, retention time, retention index, mass-to-charge ratio, and signal intensity. In each sample, all peak signal intensities were segmented and normalized according to the internal standards with an RSD greater than 0.3 after screening. After the data was normalized, redundancy removal and peak merging were conducted to obtain the data matrix.

The matrix was imported in R to carry out Principal Component Analysis (PCA) to observe the overall distribution among the samples and the stability of the whole analysis process. OPLS-DA and PLS-DA were utilized to distinguish the metabolites that differ between groups. To prevent overfitting, 7-fold cross-validation and 200 Response Permutation Testing (RPT) were used to evaluate the quality of the model.

VIP values obtained from the OPLS-DA model were used to rank the overall contribution of each variable to group discrimination. A two-tailed Student's *t*-test was further used to verify whether the metabolites of difference between groups were significant. Differential metabolites were selected with VIP values greater than 1.0 and *P*-values less than 0.05.

2.17. Cell culture and reporter gene assays

HEK293T cells were maintained in DMEM with 10% FBS. Reporter gene assay was carried out as described previously[53]. For reporter gene assays, the expression plasmids pSG5-hPXR/CYP3A4-Luc, or pcDNA3.1-hCAR/CYP3A4-Luc were cotransfected with pREP7. For transfection, each well contained 150 ng of total plasmids and 0.25 μL of FuGENE HD transfection reagent (Roche, Germany) for 24 h. Then, hPXR, hCAR agonist (Rifampicin and CICTO respectively), and metabolites (glycerol monosterate, palmitoyglycine, *R*-3-hydroxybutyric acid, sarcosine, talniflumate) were added to fresh media and incubated 24 h. The luciferase activity was measured using the Dual-Luciferase Reporter Assay System (Promega, USA), and the transfection efficiencies were and normalized according to *Renilla* luciferase activity.

2.18. RNA extraction and RT-qPCR

Real-time quantitative PCR was performed as mentioned previously[54]. Briefly, total RNA was isolated from more than 10,000 nematodes or the liver using the Trizol reagent (Vazyme, Nanjing, China) according to the manufacturer's instructions under RNase-free conditions. One μg of total RNA was used as the template to synthesize cDNA with a cDNA kit (Vazyme, Nanjing, China). RT-qPCR was performed under the following conditions: 42 °C for 2 min, 50 °C for 15 min, and 85 °C for 5 s with ChamQ Universal SYBR qPCR Master mix (Vazyme, Nanjing, China) on an ABI StepOne Plus real-time PCR system (Applied Biosystems, USA). *β*-Actin was used as the internal reference for the expression level of all genes. Statistical analysis was carried out by using $2^{-\Delta\Delta Ct}$ method. The sequences of all primers are listed in Supporting Information Tables S1 and S2.

2.19. Western blotting analysis

The protein was extracted from the liver tissues using RIPA buffer (Beyotime, Shanghai, China) containing protease inhibitor, phosphatase inhibitor, and phenylmethylsulfonyl fluoride (PMSF). The 30 μg of proteins were separated using sodium dodecyl sulfate-polyacrylamide (SDS-PAGE) gel, and transferred to polyvinylidene fluoride (PVDF) membranes. Blocked in 5% BSA for 2 h at room temperature, and incubated in primary antibodies for GSTA1, CYP1A1, CYP51A1, CYP3A11 (Proteintech, Wuhan, China), and GAPDH (Huabio, Hangzhou, China), with 1:1000 dilution in 3% BSA at 4 °C overnight. Then, the membranes were washed three times with TBST each 10 min, and incubated in the secondary antibody at room temperature for 2 h. The blots were visualized using an ECL chemiluminescence kit (Beyotime, Shanghai, China). GAPDH was used as a loading control, and Image J software (National Institutes of Health, Bethesda, MD, USA) was used for densitometric analysis of the bands.

2.20. Statistical analysis

Statistical analyses were performed using GraphPad Prism V.7.0.0 (La Jolla, CA, USA) and SPSS (version 21.0). All data were presented as means ± Standard error of mean (SEM). Comparisons were carried out *via* one-way analysis of variance (ANOVA), two-way (ANOVA), and two-tailed unpaired Student's *t*-test. Differences were considered statistically significant when P was <0.05.

3. Results

3.1. OCA prolongs lifespan and enhances fitness in C. elegans

To investigate whether the activation of FXR can extend lifespan, 5 identified FXR agonists were used to assay the lifespan of *C. elegans*. Of which, 5 compounds, including GW4064, OCA, ITG, 27-hydroxymangiferolic acid, and mulberrin, exhibited significant longevity promotion activities (Fig. 1A−E and Supporting Information Table S3) in wild-type N2 worms. Since OCA is a potent FXR agonist, thus we focused on the effects of OCA on aging. We found OCA significantly promoted the lifespan of the worms. As shown in Fig. 1F, OCA prolonged the lifespan of *C. elegans* from 19.32 days to 21.80 days, 22.71 days, and 23.56 days (10.53%, 15.79%, and 21.53% compared to the control group) at 5, 10, and 20 μmol/L in a dose-dependent manner with EC_{50} value of 2.721 μmol/L. However, when the concentrations of OCA were increased to 50 and 100 μmol/L, the lifespan-extending effect of OCA was attenuated, which was consistent with a previous finding[55], suggesting that higher concentration of OCA may have off-targeting effects on worms.

Dietary restriction is one of the well-known approaches to extend worm lifespan[56]. It can be induced when a compound inhibits bacterial growth, thereby reducing the amount of food available or acting as a repellent for the worms and inhibiting food intake[57]. To determine the aging retarding effects on *C. elegans* that did not result from inhibiting bacteria growth and food intake, we measured the effect of OCA on bacteria *E. coli* OP50 growth following OCA treatment. As shown in Supporting Information Fig. S1A, OCA treatment did not affect bacteria growth. In addition, worms did not avoid bacteria treated with OCA (Fig. S1B and S1C). These results indicate that OCA extending lifespan is not by affecting bacteria availability and food intake. Notably, OCA also increased worm lifespan as compared with the vehicle group when fed bacteria killed by heating (Fig. 1G). Together, these data demonstrate that OCA-mediated lifespan extension occurs by a direct action on *C. elegans* rather than dietary change.

C. elegans showed a behavioral and physiological decline with age like mammals. With aging progress, *C. elegans* exhibited a decline in maximum velocity, pharyngeal pumping rate, and sarcopenia[32,33]. We next evaluated the effect of OCA on worm activity, and the results showed that both pharyngeal pumping rate and body bending were significantly improved by OCA treatment from L1 and L4 stages compared to the vehicle group (Fig. 1H−K). Notably, a higher dose of OCA (50 μmol/L) did not better ameliorate effects on pumping rate and body bending than a lower dose (10 μmol/L), confirming that a low dose of OCA was effective on fitness (Fig. S1D and S1E). Furthermore, the pumping rate also reflected the food intake of nematodes, corroborating that the lifespan extension of OCA is independent of food intake (Fig. S1A−S1C). Then we explored the motion of the nematodes and found that OCA enhanced the mobility of the nematodes (Fig. 1L). These data indicate that OCA may also improve healthspan during the aging process. Lifespan extension is often caused by reduced fertility or delayed development[58]. Thus, we analyzed the fecundity of the wild-type worms and found that after OCA treatment, the number of eggs had no significant difference between the vehicle and OCA group, indicating that the lifespan extension effect of OCA was not due to the reproductive inhibition (Fig. S1F).

3.2. OCA extends lifespan through insulin/insulin-like growth factor-1 signaling (IIS) pathway

The IIS signaling pathway is an important regulator of metabolism, development, growth, fecundity, and stress resistance[59]. In *C. elegans*, insulin/IGF-1 transmembrane receptor (IGFR) ortholog DAF-2 regulates transcription factor FOXO ortholog DAF-16, which regulates most of the functions of the IIS pathway through several kinases[5]. Reduced IIS signaling during adulthood or at an advanced age is sufficient to extend lifespan[60]. To determine whether OCA mediates lifespan expansion depending on IIS signaling, we assayed the lifespan of *daf-16*-null mutant, *daf-16* (*mu86*) worms after treatment with OCA. The results showed that OCA failed to extend the survival rates of the *daf-16* (*mu86*) mutant, unlike in N2 worms (Fig. 2A and B and Table S3), suggesting that OCA's longevity-expanding effects require DAF-16 action. To confirm this, we assayed the effects of OCA on DAF-16 nuclear translocation and its transactivity. The findings revealed that OCA induced DAF-16::GFP nuclear translocation (Fig. 2C) and upregulated the expression of its downstream genes, including *sod-2*, *sod-3*, *clk-1*, *unk-48*, *pha-4*, *hsp16.2* and *sir-2.1* (Fig. 2D).

Then, we examined the roles of other IIS pathway molecules in OCA-induced lifespan extension. Indeed, when *daf-2* (*e1370*) worms were treated with OCA, there were similar mean and maximal survival rates as vehicle treatment (Fig. 2E and Table S3). In addition, *age-1* (phosphatidylinositol-3-OH kinase catalytic subunit) is the first longevity gene found in *C. elegans*[61]. We found that similar to that of *daf-16* (*mu86*) and *daf-2* (*e1370*) mutants, the lifespan of the *age-1* (*hx546*) mutant was not extended by OCA treatment (Fig. 2F and Table S3). These data indicate that the lifespan extension effect of OCA may be related to the IIS pathway to some extent.

Longevity is also related to oxidative and heat stress[62,63], and the activity of stress resistance is beneficial to the survival of animals. Next, we measured the survival rates of worms under heat stress and oxidative stress. L4 worms were treated with OCA for 5 consecutive days at 20 °C and then subjected to 35 °C incubators for heat stress or 8 mmol/L H_2O_2 for oxidative stress analysis. As concluded in Fig. 2G and H, and Supporting Information Table S4, under heat stress, the survival rates increased from 7.26 to 9.00 h (a 23.7% increase compared to the control group) after the treatment of OCA (Fig. 2G). While, under oxidative stress, the survival rates increased from 4.37 to 5.70 h (a 30.43% increase compared to the control group) after OCA treatment (Fig. 2H). Taken together, these data indicate that OCA can enhance stress resistance.

3.3. OCA upregulates the xenobiotic detoxification genes in C. elegans

To investigate the underlying mechanisms of OCA in longevity, we analyzed genome-wide gene expression through RNA-seq analysis in worms to clarify the potential pathways and genes mediating the aging-extending action of OCA. Principal component analysis (PCA) showed a separation of transcriptomes associated with these different phenotypes between the vehicle and OCA-treated group (Fig. 3A). As shown in Fig. 3B, following 3 days of OCA treatment, 124 genes were upregulated, and 345 genes were downregulated which showed in volcano plot (fold change >2, FDR <0.05). A large number of GO terms were enriched in upregulated

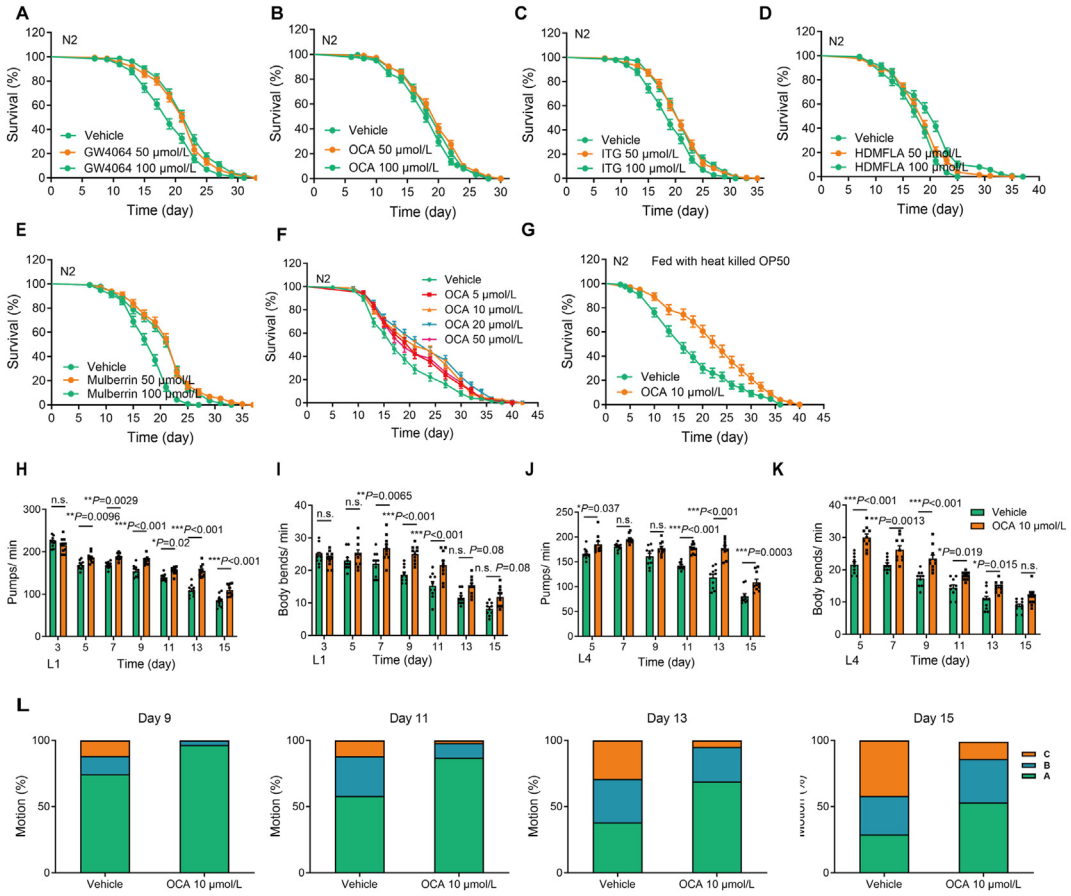

Figure 1 OCA extends lifespan and enhances fitness in *C. elegans*. Representative survival curves of FXR agonists, including (A) GW4064 at dose of 50 and 100 μmol/L; (B) 50 and 100 μmol/L OCA; (C) 50 and 100 μmol/L ITG; (D) 50 and 100 μmol/L 27-hydroxymangiferolic acid; (E) 50 and 100 μmol/L mulberrin. GW4064, low dose OCA, ITG, 27-hydroxymangiferolic acid, mulberrin extended lifespan compared to the vehicle (log-rank test, $n = 138-187$). (F) Survival curves of worms treated with different dose of OCA (log-rank test, $n = 142-150$). (G) Survival curves of worms maintained on heating-killed OP50 bacteria treated with 10 μmol/L OCA or vehicle (log-rank test, $n = 102-129$), and dead OP50 was obtained through 65 °C incubation for 4 h. (H, I) The pharyngeal pumping rate and body bending rate of worms treated with OCA from L1 stage ($n = 10$ in each group). The pump rate and body bend rate within 1 min was recorded on Days 3, 5, 7, 9, 11, 13 and 15. The synchronized worms were transferred to the plate pretreated with or without OCA after 24 h incubation at 20 °C container. (J, K) The pharyngeal pumping rate and body bending rate of worms treated with OCA from L4 stage ($n = 10$ in each group). The pump rate and body bend rate within 1 min was recorded on Days 5, 7, 9, 11, 13 and 15. The synchronized L1 worms were transferred to the plate pretreated with OP50, and then transferred worms to the plate pretreated with or without OCA at L4 stage. (L) The motion of worms treated with OCA. The effect of OCA on motion counted on Days 9, 11, 13, and 15. Motion was classified into three groups, Motion A: nematodes moved freely, Motion B: nematodes moved slowly after stimulation, Motion C: nematodes only moved head and tail after prodding. $n = 50$ nematodes in each group each time. All lifespan was carried out at 20 °C. See Table S3 for detailed statistical analysis of lifespan data. Significance was analyzed by (H–K) two-way ANOVA. All data are presented as mean ± SEM. Compared with vehicle group, $^{*}P < 0.05$, $^{**}P < 0.01$, $^{***}P < 0.001$. n.s., not significant. OCA, obeticholic acid; ITG, Isotschimgine; HDMFLA, 27-hydroxymangiferolic acid.

genes, including cellular, metabolic, biological regulation process, structural molecular activity, catalytic activity, and transporter activity, etc (Fig. 3C). Interestingly, through the top 20 of Kyoto Encyclopedia of Genes and Genomes (KEGG) pathway enrichment analysis, we functionally classified the pathways including drug metabolism-cytochrome P450 and other enzymes, xenobiotics metabolism by cytochrome P450, biosynthesis of cofactors, etc (Fig. 3D). To validate the effect of OCA on the regulation of genes enriched in the KEGG pathways, we assayed the genes expression levels in worms using qRT-PCR. We found that OCA treatment upregulated the detoxifying genes' mRNA levels, including *gst-4*, *gst-10*, and *ugt-55* (Fig. 3E). The data indicate that OCA may increase detoxification gene expression, a common transcriptome marker of most longevity interventions[20].

Xenobiotic toxicants were detoxified through a three-step procedure. The phase I detoxification enzymes, such as CYPs, chemically modify toxins and then bind to phase II enzymes, making them more water soluble[64]; finally, these modified toxins are secreted out of the cells by ABC transporters[65]. In the qRT-PCR analysis, we found that several genes involved in xenobiotic detoxification, including *cyp13a1*, *cyp14a1*, *cyp14a3*, *cyp35a3*, *cyp35a5*, *cyp35b1*, *cyp35b3*, *cyp35c1*, *cyp36a1*, *gst-4*, *gst-10*, *ugt-44*, *pgp-3*, and *pgp-14*, were transcriptionally upregulated in worms after OCA treatment (Fig. 3F). To further determine whether the depletion of detoxification genes would affect the lifespan of worms, *cyp35a3*, *cyp35b3*, *gst-4*, *gst-10*, *ugt-44*, and *pgp-3* were suppressed using RNA interference in N2 worms. The results showed that the maximum day of survival in

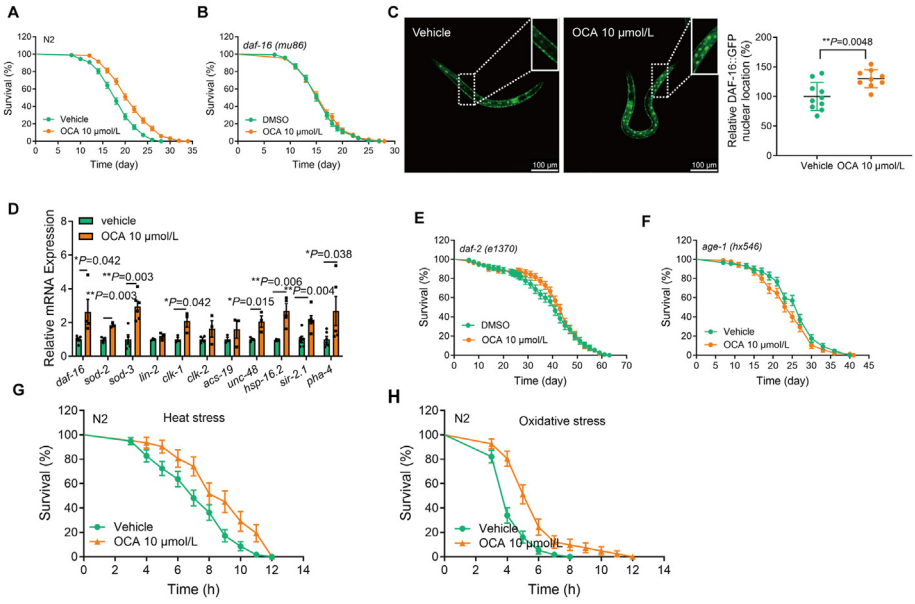

Figure 2 IIS pathway is involved in OCA mediated lifespan extension. (A) The survival curve of wild type worms. (B) The survival curve of *daf-16 (mu86)*. (C) The nuclear translocalization of DAF-16::GFP (*muIs 109*) worms. At least 10 worms were analyzed. Scale bar, 100 μm. (D) The expression of the downstream genes of *daf-16* tested by RT-qPCR. (E) The survival curve of *daf-2* (*e1370*). (F) The survival curve of *age-1* (*hx546*). n = 106−146 nematodes for each group (A−B, E−F). Lifespans were performed at 20 °C, and analyzed by log-rank test. The data are expressed as mean lifespan ± SEM. The detailed lifespan data were listed in Table S3. (G) Survival curves of nematodes under 35 °C for heat stress analysis (n = 30−58 nematodes for each group each time, experiment repeated 3 times). (H) Survival curves of nematodes exposed to hydrogen peroxide (final concentration: 8 mmol/L) for oxidative stress analysis (n = 40−60 nematodes for each group each time, experiment repeated 3 times). The survival data were analyzed by log-rank test, and the detailed data are concluded in Table S4. Significance was analyzed by two-tailed unpaired Student's t-test (E, F). Data are presented as mean ± SEM. Compared with vehicle group, $^*P < 0.05$, $^{**}P < 0.01$. OCA, obeticholic acid.

the vehicle group in c*yp35a3*, *cyp35b3*, *gst-4*, *gst-10*, *pgp-3*, and *ugt-44* knockdown worms was shorter than that in the control RNAi (Ev) group (Fig. 3G−M and Supporting Information Table S5). The median lifespan of c*yp35a3* and *cyp35b3* was only 11 days and 9 days, respectively, which was also shorter than that in the Ev group. After the treatment of OCA, the lifespan in those lines was not extended compared to that in the Ev group. Collectively, these data suggest that OCA may extend lifespan through upregulating detoxification genes.

3.4. OCA activates the xenobiotic detoxification machinery via conserved transcription factors in C. elegans

The expression of detoxification genes is regulated by evolutionarily conserved transcription regulators[15] such as NHRs[66-68]. Given OCA upregulates detoxification genes (Fig. 3), we hypothesized that OCA may activate NHRs to upregulate the detoxification machinery. In *C. elegans*, NHRs are mainly involved in xenobiotics metabolism, including DAF-12, NHR-8, and NHR-48, structurally and functionally related to FXR, PXR, and CAR in mammals[69-71]. The gene expression analysis showed that the expression of xenobiotic detoxification genes was diminished in *nhr-8* (*tm1800*) and *daf-12* (*rh61rh411*) mutants (Supporting Information Fig. S2A and S2B). Next, we asked whether the lifespan-extending effects of OCA require NHR-8 and DAF-12 signaling in worms. We found that unlike in N2 worms, in *nhr-8* (*tm1800*) mutant, OCA treatment did not result in increased lifespan compared to vehicle treatment (Fig. 4A and B and Table S3), and similar results were observed in *daf-12* (*rh61rh411*) mutants (Fig. 4C and Table S3). These data indicate that the longer lifespan after OCA treatment may rely on the activation of NHR-8 and DAF-12 signaling.

Multiple global transcriptional regulators like FOXO/DAF-16 and NRF2/SKN-1 are important for longevity[8,72]. We then evaluated whether DAF-16 was involved in NHR-8 and DAF-12 signaling and found that the nuclear translocation in intestinal cells was diminished in *nhr-8* (*tm1800*) or *daf-12* (*rh61rh411*) crossed with DAF-16::GFP worms (Fig. 4D and E). These data suggest that DAF-16 may coordinate with NHR-8 and DAF-12.

To further examine whether the lifespan-extending effect of OCA was related to xenobiotic toxins detoxification, we exposed worms to PQ, MeHgCl, CC and CQ, which were identified to impair lifespan and healthspan. As shown in Fig. 4F−I, when exposed to PQ, MeHgCl, CC, and CQ, the survival rates of N2 worms were reduced, while OCA treatment rescued the survival rates in a dose-dependent manner. In contrast, the rates of death of *daf-12* and *nhr-8* mutant worms were higher than those in N2 worms at the same point after exposure to the toxins, indicating that OCA might improve lifespan through NHR-8 and DAF-12 mediated detoxification effects. In addition, we measured the cell viability of L02 cells after exposure to PQ, MeHgCl, CC, and CQ to assay whether OCA could enhance the detoxification function in human hepatocytes. We found that L02 cell viability was rescued by OCA when exposed to PQ, CQ, and CC, but not MeHgCl (Fig. S2C−S2F). Together, these data indicate that an activated xenobiotic detoxification system is essential for OCA to extend its lifespan.

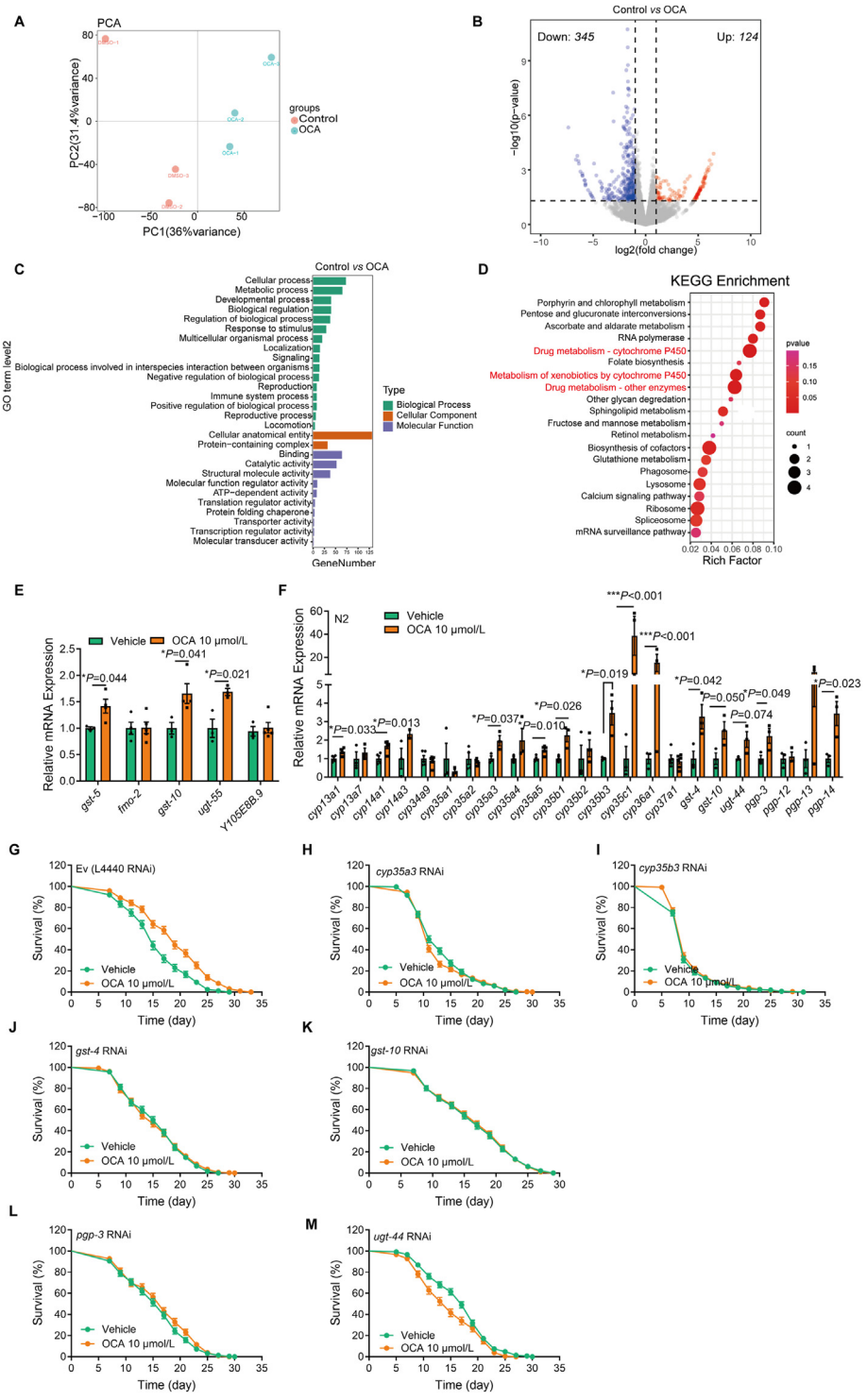

Figure 3 OCA increases the expression of detoxifying genes in *C. elegans*. (A) Principal component analysis (PCA) of samples with or without OCA treatment. (B) Volcano plot analysis of samples. (C) Gene ontology (GO) terms that are enriched in control and OCA group worms. (D) The Kyoto Encyclopedia of Genes and Genomes (KEGG) analysis of enriched pathways in OCA-treated *C. elegans*. (E) qRT-PCR analysis of differential genes in RNA-seq. (F) Transcription levels of phase I, II xenobiotic enzymes and ATP transporters in wild type worms treated with OCA. The gene expression was analyzed by RT-qPCR. $n \geq 3$ in each group. The lifespan of worms fed with control RNAi bacteria L4440 (G), *cyp35a3* (H), *cyp35b3* (I), *gst-4* (J), *gst-10* (K), *pgp-3* (L) and *ugt-44* (M), $n = 161-287$ nematodes for each group. The lifespan assay was performed at 20 °C, and analyzed by log-rank. Data are expressed as mean lifespan ± SEM, and the detailed lifespan results were listed in Table S5. (E, F) were analyzed by Two-tailed unpaired Student's *t*-test. Data are expressed as mean ± SEM. Compared with vehicle group, $^*P < 0.05$, $^{***}P < 0.001$. n.s., not significant. OCA, obeticholic acid.

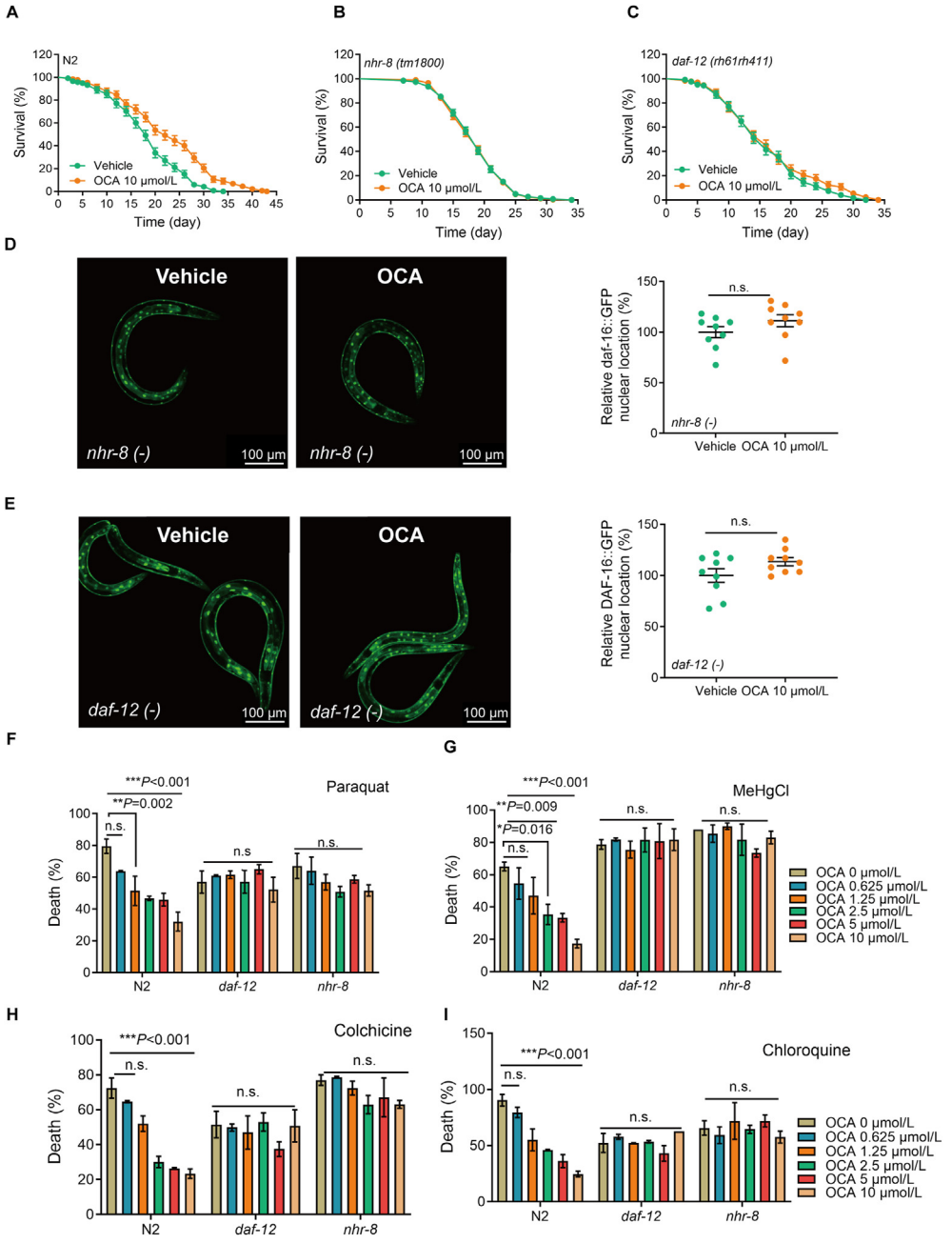

Figure 4 Xenobiotic detoxification is required for OCA induced longevity. The survival curves of N2 worms (A), *nhr-8* (*tm1800*) (B), and *daf-12* (*rh61rh411*) (C) treated with OCA. All lifespans were performed at 20 °C and analyzed by log-rank, $n = 123-264$. The detailed lifespan data are expressed in Table S3. (D) The nuclear translocalization of *nhr-8* (*tm1800*) crossed with DAF-16::GFP. Scale bar, 100 μm. (E) The nuclear translocalization of *daf-12* (*rh61rh411*) crossed with DAF-16::GFP. Scale bar, 100 μm. At least 10 worms were used to analyze. (F) The toxic resistance of N2 worms, *daf-12* and *nhr-8* mutants to 200 mmol/L paraquat (PQ). About 50 worms in each dose of OCA. (G) The survival rate of N2, *daf-12* and *nhr-8* worms treated by 2 μmol/L MeHgCl. (H) The livability of N2, *daf-12* and *nhr-8* mutant exposed to 4 mmol/L colchicine (CC). (I) The livability of N2, *daf-12* and *nhr-8* mutants exposed to 4 mmol/L chloroquine (CQ). Significance was analyzed by two-tailed unpaired Student's *t*-test (D, E); One-way ANOVA (F, G, H, I). Data are expressed as mean ± SEM. and $n \geq 3$ in each experiment. Compared to vehicle group, $^{*}P < 0.05$, $^{**}P < 0.01$, $^{***}P < 0.001$. n.s., not significant. OCA, obeticholic acid. MgHgCl, methylmercury chloride.

3.5. The lipid metabolism might be involved in the lifespan-extending effect of OCA

FXR regulates fatty acid synthesis and desaturation, sterol metabolism, and bile acid transport, thus coordinating lipid and cholesterol metabolism[73]. In *C. elegans*, FAT-2 (Δ12 desaturase) and FAT-3 (Δ6 desaturase) were responsible for the transform monounsaturated fatty acids to polyunsaturated fatty acids, and FAT-5, FAT-6, and FAT-7 (Δ9 desaturase) could transform the saturated fatty acids to monounsaturated fatty acids. To answer whether lipid metabolism is involved in lifespan-extending effects of OCA in *C. elegans*, we performed the lifespan assays in the

fatty acid desaturases enzyme deficient worms, including *fat-2* (*wa17*), *fat-3* (*ok1126*), *fat-5* (*tm420*), *fat-6* (*tm331*) and *fat-7* (*wa36*) mutants. We found that when FAT genes were blocked in nematodes, the lifespan-extending effects of OCA were diminished (Fig. 5A−F and Table S3).

AMPK and mTOR are two important hubs to regulate energy homeostasis. The activation of AMPK and the inhibition of mTOR can extend lifespan and reduce stress resistance[74-76]. The results showed that the lifespan-extending effect of OCA was also suppressed in *aak-2* (*ok524*), the homolog gene of AMPK, mutant worms (Fig. 5G and Table S3). Meanwhile, the lifespan of *let-363* (*ok3018*) mutant, the homolog of TOR, and *raga-1* (*ok386*), a gene encoding a homologous protein to RagA, which senses amino acids and activates TORC1, did not extend after OCA treatment (Fig. 5H and I, and Table S3). Dietary restriction (DR)[77], and *sir-2.1*, the SIRT1 homolog in humans, deletion or knockdown of the gene shorted the lifespan[78]. The survival rate did not increase in *eat-2* (*ad1116*), mimics DR, and *sir-2.1* (*ok434*) mutants (Fig. 5J and K and Table S3).

Mitochondrial metabolism is important in mediating longevity, and mitochondrial dysfunction is sufficient to induce aging[79]. Mitochondria dysfunction is a hallmark of aging, and crucial in cellular metabolism and ATP production[80]. Therapeutic interventions on aging can target mitochondria biogenesis, including manipulating cellular chemistry and energy homeostasis[81,82]. To explore the energy homeostasis in OCA-treated worms, *myo-3p::TOMM-20::mKate2::HA* (*foxSi16*) worms were used to test the mitochondrial homeostasis. We monitored young (Day 1) and old (Day 10) worms treated with OCA starting from the L4 stage for mitochondrial content. In young worms, OCA treatment resulted in comparable mitochondrial content in muscle cells compared with vehicle treatment (Fig. 5L). In contrast, old worms exposed to OCA had higher mitochondrial integrity compared to the vehicle group (Fig. 5M), suggesting that OCA may improve mitochondrial homeostasis in older worms. These data indicate that regulating lipid metabolism and energy homeostasis might be involved in OCA extending lifespan.

3.6. *OCA activates detoxification machinery in mice*

The liver is the major detoxification organ[83]. Recently, it has been identified that 17 known lifespan-extending interventions may induce common transcriptome markers including an increase in the expression of detoxification genes in the liver of mice, which could be used to predict new longevity therapy[20]. To investigate the transcriptome in the liver of mice, the mice were treated with or without OCA, and the liver tissues were analyzed by RNA-sequence technique. Volcano plot showed that there were 143 genes were upregulated, and 223 genes were downregulated after OCA treatment (Fig. 6A). GO terms, including biology process, molecular function, and cellular component, showed that cellular process, metabolic process, biological regulation, cellular anatomical entity, intracellular, binding, catalytic activity, and detoxification were enriched (Fig. 6B).

Previously, several reports showed that longevity interventions displayed the same transcriptome markers of enhanced detoxification gene expression in the livers of mice[20]. As shown in Fig. 6C, KEGG enrichment analysis showed that drug metabolism through cytochrome P450 enzymes, glutathione metabolism, and xenobiotics metabolism pathways were highly correlated with the enriched pathways in *C. elegans* (Fig. 3D). To further identify pathways associated with detoxification and longevity, functional gene set enrichment analysis (GSEA) indicated that xenobiotics metabolism and drug metabolism by cytochrome P450 were upregulated after OCA treatment (Fig. 6D−F). Meanwhile, OCA treatment inhibited cellular senescence (Fig. 6G) and insulin signaling pathway (Fig. 6H). And then the expression of differentiate genes was validated by RT-qPCR, and found that OCA treatment upregulated the expression of genes associated with drug/xenobiotics metabolism and other pathways, including *Gstm3*, *Gstm7*, *Cyp2c55*, *Ugt2b5*, *Ugt1a1*, and *Gpx-1* in the liver of mice (Fig. 6I). Together, these results suggest that OCA may upregulate the expression of drug/xenobiotic metabolism genes in mice.

3.7. *OCA improves Dox-induced early senescence via upregulation of detoxification functions in mice*

Dox is a chemotherapeutic drug that can induce early senescence and other long-term health conditions in patients and rodents, and has been widely used to induce accelerated aging models[84,85]. Thus, we performed lifespan and healthspan assays to test whether OCA could counteract the senescence-accelerating effects of Dox in mice. In the lifespan assay, the mice were administrated with Dox and OCA until the last mice died. Notably, OCA extended the mean lifespan of Dox-induced mice from 19 days to 45 days (a 139% increase) compared to the Dox group (Fig. 7A and Supporting Information Table S6). In the healthspan assay, the procedure of Dox-induced aging mice was listed in Fig. 7B. Dox decreased body weight, and OCA did not reverse this change (Supporting Information Fig. S3A). The climbing down time from the pole test and the passing time spent on the balance beam was elevated in the Dox group (Fig. 7C and D), while OCA reduced the time of T-climbing and passing time (Fig. 7C and D), suggesting that OCA could improve the motor ability in Dox-induced premature mice. At the end of the healthspan experiment, the serum was collected, and the level of ALT and AST, the markers of liver injury, were analyzed. We found Dox treatment led to the elevation of ALT and AST levels (Fig. 7E and F) and an increase in inflammatory cell infiltration (Fig. 7G and H). Interestingly, OCA reduced ALT and AST levels and inhibited inflammatory cell infiltration in Dox-induced aging mice (Fig. 7E−H). The expression of the pro-aging factors, including *p16*, *p21*, and *p53* was increased in the liver of Dox-induced mice, while OCA reduced their expression (Fig. 7I). The increase in Senescence Associated Secretory Phenotype (SASP) is another marker of aging cells and tissues, including IL-6, IL-1β, TNF-α, MMP-3, etc. The mRNA analysis showed that OCA downregulated the gene expression of *Il-6*, *Il1b*, and *Tnfa* in the liver of Dox-treated mice (Fig. 7I). The data indicate that OCA treatment could reverse pro-aging-related factors transcriptionally which is consistent with previous findings of FXR inhibiting inflammation[86]. Furthermore, as shown in Fig. 7J and K, Masson trichrome staining showed that the collagen accumulation in the heart induced by Dox was reversed by OCA treatment. Moreover, the liver tissues were stained by Sirius red and Masson trichrome. The results showed that OCA alleviated hepatic fibrosis in mice induced by Dox (Fig. S3B−S3E). These data indicate that OCA might protect the liver and the Dox-induced heart damage. To investigate whether OCA could regulate the detoxification gene expression in the liver of Dox-treated mice, we carried out RT-qPCR. The results showed that OCA upregulated the expression levels of *Gstm3*, *Cyp2c55*, *Ugt1a1*, *Gstm2*, *Cyp2c29*, *Gstt3*, and *Gpx-1* (Fig. 7L), which is consistent with previous findings (Fig. 6). Meanwhile, Western blot analysis

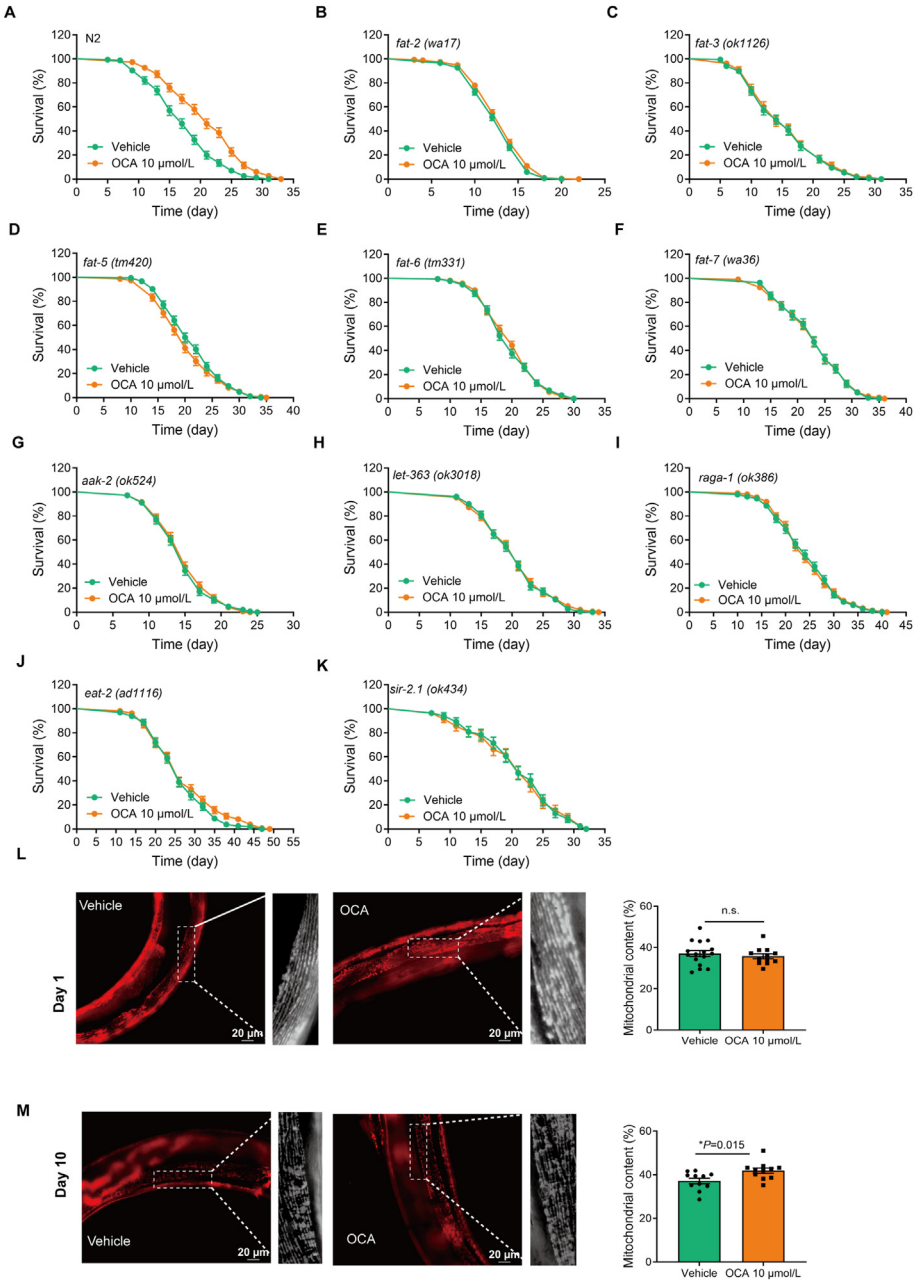

Figure 5 The lipid metabolism may be involved in the lifespan-extending effect of OCA. Survival curves of wild type worms (A), *fat-2* (*wa17*) (B), *fat-3* (*ok1126*) (C), *fat-5* (*tm420*) (D), *fat-6* (*tm331*) (E), and *fat-7* (*wa36*) mutants (F). The survival curve of *aak-2* (*ok524*) (G), *let-363* (*ok3018*) (H), *raga-1* (*ok386*) (I), *eat-2* (*ad1116*) (J) and *sir-2.1* (*ok434*) (K) mutant. $n = 106-319$ nematodes for each group. Lifespan assays were performed at 20 °C except *fat-2*, which was maintained at 25 °C, and all lifespan assays were analyzed by log-rank test. Data were expressed as mean lifespan ± S.E.M. The detailed lifespan results are listed in Table S3. (L) Representative images and RFP quantification of mitochondrial content on Day 1 of adulthood in muscle (p_{myo-3} mtRFP) mito::RFP reporter strains ($n \geq 10$). Scale bar, 20 μm. (M) Representative images and RFP quantification of mitochondrial content on Day 10 of adulthood in muscle (p_{myo-3} mtRFP) mito::RFP reporter strains treated with OCA or vehicle, ($n \geq 10$). Scale bar, 20 μm. The data are analyzed by two-tailed unpaired Student's *t*-test. Compared to vehicle group, $^*P < 0.05$. n.s., not significant. OCA, obeticholic acid.

showed that GSTA1, CYP1A1, CYP3A11 and CYP51A1 protein levels were induced by OCA treatment (Fig. 7M and Fig. S3F−S3I). In humans, CYP3A4 is the predominant CYP3A isoform, while in rodents, analogous isoforms include CYP3A1/2 in rats and CYP3A11 in mice. Given that FXR regulates bile acid metabolism, FXR downstream genes were measured. The data show that OCA upregulated *Shp*, *Bsep*, and *Sult2a1* expression and reduced the expression of *Cyp7a1*, an *Shp* downstream gene and a negative regulator of bile acid synthesis (Fig. S3J). Taken together, these data suggested that OCA could improve the healthspan and extend the lifespan induced by Dox through activating the xenobiotic detoxification action in mice.

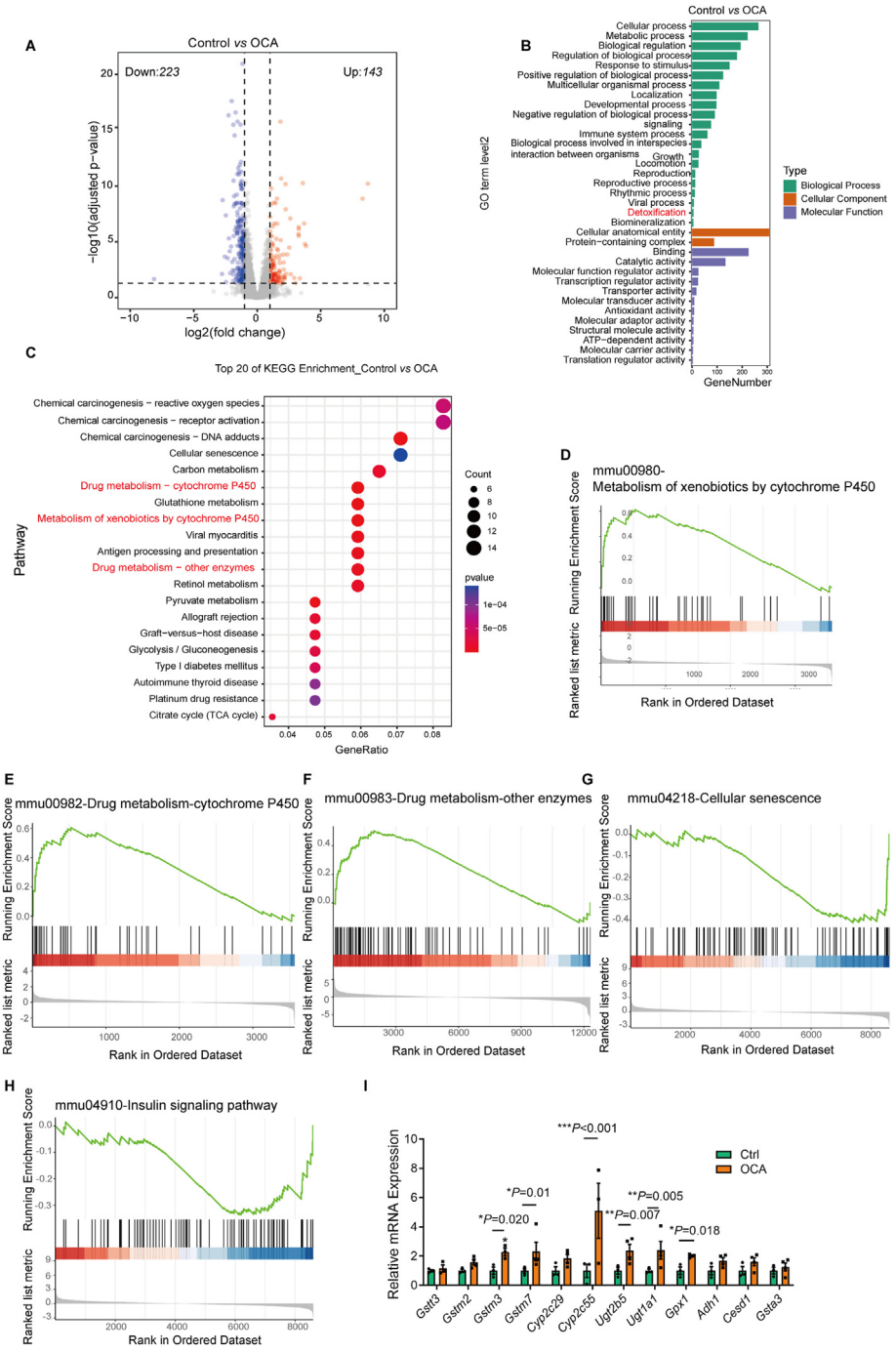

Figure 6 OCA activates detoxification machinery in mice. (A) Volcano plot analysis of the samples. (B) Gene ontology (GO) terms that are enriched in control and OCA group mice, including biological process, cellular component and molecular function. (C) The Kyoto Encyclopedia of Genes and Genomes (KEGG) analysis of enriched pathways in OCA-treated mice. (D−H) Functional gene set enrichment analysis (GSEA) of metabolism of xenobiotics by cytochrome P450, drug metabolism-cytochrome P450, drug metabolism-other enzymes, cellular senescence, and insulin signaling pathway. (I) RT-qPCR analysis of genes enriched in xenobiotics and drug metabolism pathways ($n = 4$). Significance was analyzed by two-tailed unpaired Student's *t*-test. Data are presented as means ± SEM. Compared with Ctrl group, $^{*}P < 0.05$, $^{**}P < 0.01$, $^{***}P < 0.001$. OCA, obeticholic acid.

3.8. The lifespan-extending effect of OCA is diminished in $Fxr^{-/-}$ mice

To determine the lifespan extension effect of OCA through activating FXR, $Fxr^{-/-}$ mice were used to assay the effects of OCA on healthspan and lifespan in Dox-treated mice. Firstly, we performed the pole test and the balance beam test to assay the motor ability of the mice and found that unlike in WT mice, OCA did not change the motor ability in $Fxr^{-/-}$ mice (Supporting Information Fig. S4A and S4B). In WT mice, the time of climbing down from

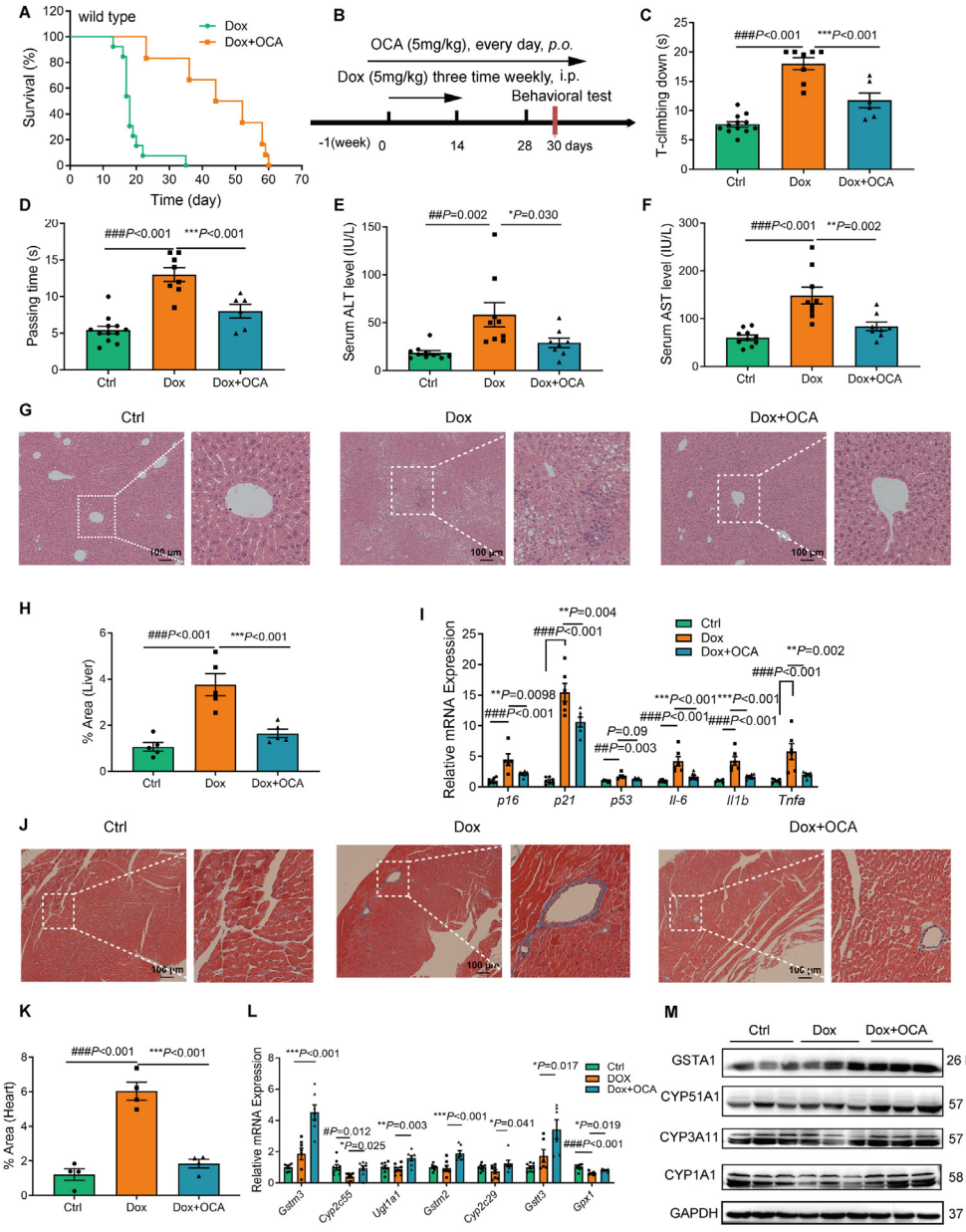

Figure 7 OCA improves the impairment of Doxorubicin (Dox)-induced premature mice. (A) The survival curves of Dox-induced mice. Dox was administrated three times weekly for 2 weeks, and then twice weekly until the last mouse died. The lifespan was analyzed by log-rank test, and the detailed lifespan analysis is listed in Table S6. (B) The healthspan assays scheme of the process of Dox-treated mice. Dox was administrated three times weekly for 2 weeks, and OCA was treated for 4 weeks ($n = 12$ in each group). (C) The time of climbing down from the pole of the pole test. (D) The passing time spent on the balance beam. (E) The serum ALT level. (F) The serum AST level. (G) The histology of the liver tissue stained by H&E staining. Scale bar, 100 μm. (H) The quantification of inflammatory infiltration in the liver tissue by Image J software. (I) The genes expression related with pro-aging and SASP in the liver of Dox-induced mice. $n \geq 5$ in each group. (J) Masson trichrome staining of the heart tissue. Scale bar, 100 μm. (K) The quantification of collagen accumulation in the heart quantified by Image J. (L) The expression of detoxification genes by RT-qPCR. (M) Representative images of CYP1A1, CYP3A11, CYP51A1, and GSTA1 protein. $n = 3$ in each group. Significance was analyzed by One-way ANOVA. Data are expressed as mean ± SEM and analyzed by one-way ANOVA. Compared with ctrl group, $^{\#}P < 0.05$, $^{\#\#}P < 0.01$, $^{\#\#\#}P < 0.001$; Compared with Dox group, $^{*}P < 0.05$, $^{**}P < 0.01$, $^{***}P < 0.001$. Dox, doxorubicin. SASP, Senescence Associated Secretory Phenotype.

the pole test was significantly reduced, though there was no change in $Fxr^{-/-}$ mice after OCA treatment (Fig. S4A). Meanwhile, the passing time on the balance beam was also significantly reduced in WT mice, and it had no significant difference in $Fxr^{-/-}$ mice under OCA treatment (Fig. S4B). Furthermore, we performed the lifespan assay in WT and $Fxr^{-/-}$ mice through administrated with Dox twice weekly. The result showed that OCA treatment increased the lifespan of WT mice from 34 to 48 days (a 42.19% increase), while there was no change in $Fxr^{-/-}$ mice (Fig. S4C and Supporting Information Table S7). Notably, the median lifespan of $Fxr^{-/-}$ mice was 39.62% less than that of WT mice (Fig. S4D, and Table S7). And the mean survival was

decreased by 32.59% (Fig. S4E, and Table S7). These data indicate that OCA treatment may improve healthspan and expand lifespan in mice through activating FXR *in vivo*.

3.9. OCA enhances fitness in D-gal-induced accelerated aging mice

The subacute senescence model induced by D-gal in rodents was first reported by Xu et al.[87], who found that mice constantly injected with D-gal for 7 weeks exhibited a significant signature of aging. Chronic administration of D-gal induces accelerated senescence and may be related to the increased inflammation and oxidative stress *via* accumulation of reactive oxygen species (ROS), leading to cell injury and a series of degenerative changes[88]. Oxidative damage and inflammation mediate age-related alterations in several organs such as the brain, kidney, and muscle[89].

Based on the finding that OCA treatment extended lifespan in nematodes and Dox-induced mice through detoxification action, we established a D-gal-induced accelerated aging mice model to explore the healthspan enhancement effects of OCA (Fig. 8A). Under D-gal administration, the body weight of mice among control, model and OCA treated group had no difference (Fig. 8B). At the end of the experiment, behavioral tests were performed to evaluate the motor capacity and recognition impairment induced by D-gal. D-gal induced more time turning on the ball and climbing down from the pole, and OCA shortened the time turning on the ball and climbing down from the pole (Fig. 8C and D). The rotarod test is designed to evaluate motor coordination and balance[90]. D-Gal increased the first time, and the total frequencies fell from the rotarod, OCA tended to reverse them (Fig. 8E and F). The open field test (OFT) is used to assess anxiety-like behavior[91]. To investigate whether OCA treatment could alleviate anxiety, D-gal-induced aging mice were subjected to OFT after the treatment of OCA. As illustrated in Fig. 8G−I, D-gal-induced mice had short traveled total distance in the OFT and frequencies in the center. OCA significantly enhanced total travelled distance and entries in the center. Anxiety-like behavior is also assessed by the elevated plus maze test, which consists of two open and two closed arms. We found that D-gal increased the time in the open arm and decreased the time and entries in the open arm, with the treatment of OCA, the time in the closed arm was decreased, time and entries in the open arm were increased in the open arm (Fig. 8J−M). The Y-maze test is used to measure working memory and exploration activity[92]. D-gal reduced the exploratory time in the new arm, and OCA significantly increased the exploratory time in the new arm, though there were no significant changes in frequencies in the new arm (Fig. 8N and O). Finally, we explored the novel object recognition task, which is a learning and memory paradigm in mice or rats[93]. As shown in Fig. 8P−S, D-gal administration suppressed the time and frequencies explored on the novel object for 2 h, and OCA increased the time and frequencies spent on the novel object in the short-term (2 h) but not long-term (24 h). Collectively, these results suggest that OCA could attenuate mobility and cognition impairment, and learning and memory decline in D-gal-induced early senescent mice.

Then, the impairment of hippocampus neurons was assessed by H&E staining. D-gal induced neuron damage in the CA3 region, and OCA reduced damaged neurons in the CA3 region of the hippocampus (Fig. 8T and U), which responded to the memory and learning function. To further explore whether OCA could decrease the apoptosis in hippocampus neurons, TUNEL staining was used to measure the apoptosis of neurons. The data showed that OCA treatment alleviated the apoptosis of neurons in the CA3 region of the hippocampus (Fig. 8V and W). Collectively, these data visually show that OCA could effectively decrease hippocampal neuron damage and apoptosis in D-gal-induced aging mice.

To test whether OCA could improve the damage by D-gal in the liver and the heart, H&E staining was conducted to evaluate tissue morphology. The results showed that the structure of the liver tissue in control mice had normal morphology. Hepatocytes were arranged neatly after D-gal administration, and the liver exhibited slight balloon degeneration and inflammatory cell infiltration (Supporting Information Fig. S5A and S5B). In contrast, balloon degeneration and inflammatory cell infiltration in the liver of the OCA group were ameliorated (Fig. S5A and S5B). Myocardial injury induced by D-gal is a classical model for the study of heart aging[94]. As shown in Fig. S5C and S5D, the heart tissues also showed inflammatory infiltration in D-gal-induced mice compared with the control group, while OCA improved myocardial organization, neatly arranged myocardial fiber, indicating that OCA treatment could alleviate heart injury induced by D-gal. The data suggest that OCA could improve liver and heart inflammatory cell infiltration induced by D-gal.

To explore whether OCA could also activate detoxification function in mice induced by D-gal, RT-qPCR was carried out to analyze the expression of detoxification genes in the liver of mice. The data showed that D-gal induced the mRNA expression of *p16*, the marker of aging, and apoptotic genes *p53* and *p21* in mice liver, but OCA treatment reversed this trend (Supporting Information Fig. S6A). At the same time, OCA treatment also inhibited SASP factors *Il-6* and *Tnf-α* induced by D-gal (Fig. S6A). Furthermore, Notably, OCA treatment also upregulated the expression of *Gstm3*, *Cyp2c55*, *Gstt3*, *Gstm2*, *Ugt1a1*, *Gpx-1*, and *Cyp2c29* in the liver of D-gal-induced mice (Fig. S6B), which was similar with the effects of OCA in nematodes and Dox-induced mice. As illustrated in Fig. S6C−S6F, OCA induced the protein levels of GSTA1, CYP1A1, and CYP3A11 significantly. Furthermore, the RT-qPCR data showed that OCA increased the expression of bile acid transporter genes, and exhibited a tendency to reduce the expression of bile acid synthesis genes (Fig. S6G). These data suggest that OCA treatment could alleviate early senescence through upregulating xenobiotic detoxification genes in mice induced by D-gal.

3.10. OCA extends healthspan in SAMP8 mice

SAMP8 is often used in aging research because of its spontaneous senescence and various pathobiological phenotypes[95]. Next, SAMP8 mice were used to determine the aging-extending effects of OCA (Fig. 9A). The results showed that SAMP8 mice displayed significant motor ability dysfunctions such as an increase in T-climbing, passing time, and the number of falls from the rod, and a decrease in the time dwelling on the rod when compared to the normal control SAMR1 mouse. OCA treatment reduced the time of climbing down from the pole in the pole test (Fig. 9B) and the time of passing on the beam balance (Fig. 9C), and increased the time of mice stayed on the rotarod (Fig. 9D and E). These results indicate that OCA treatment could retard the senescence of motor ability in SAMP8 mice. SAMP8 mice exhibited emotional disorders and learning and memory deficits[95-97]. Next, the open field test was used to determine the anxiety of the mice. The results showed an increased tendency to enter into the center of open field (Fig. 9F−I). To assay the memory of the mice, Y-maze was used to test the exploration behavior of the new subject. The

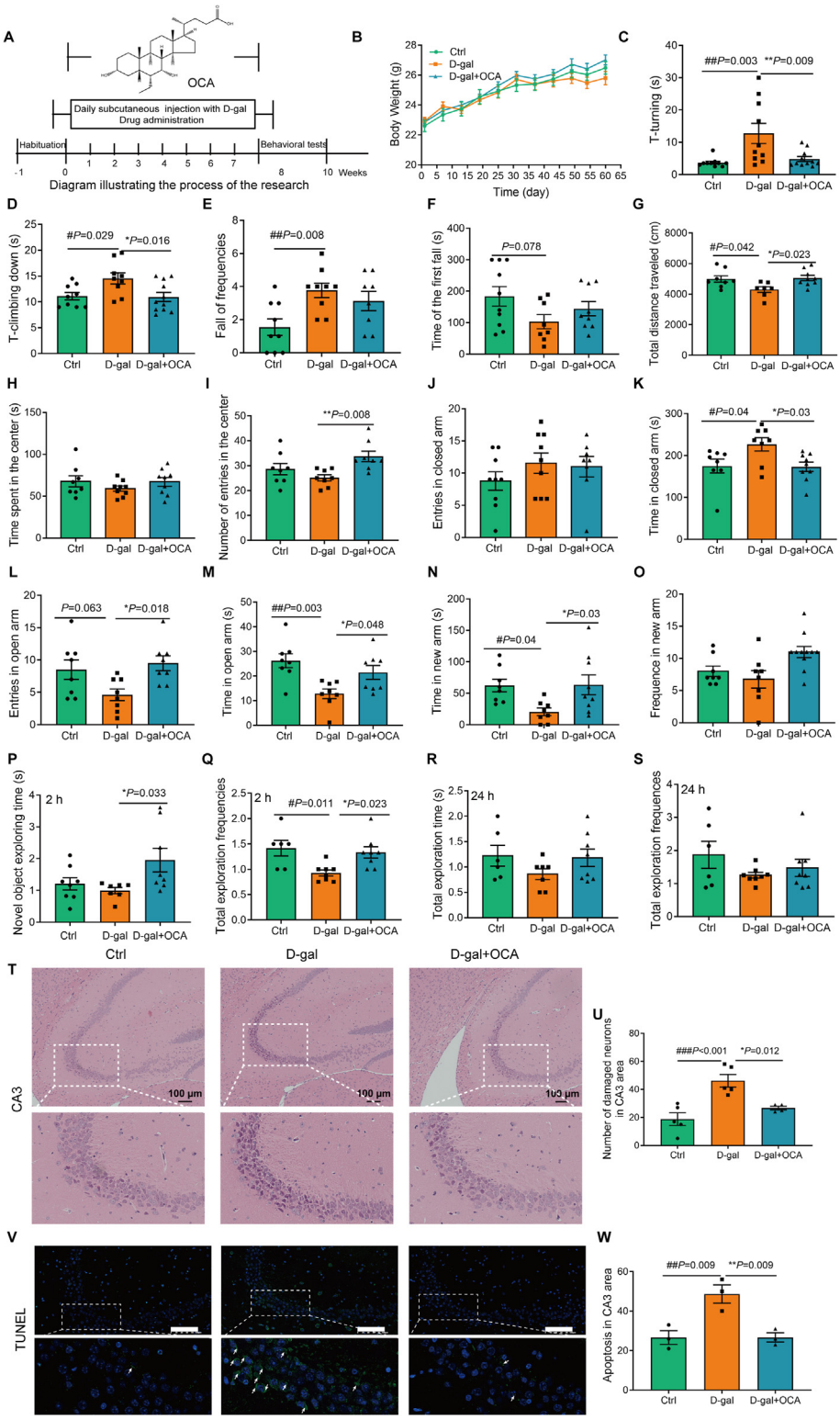

Figure 8 OCA improves healthspan in D-galactose (D-gal) induced accelerated aging mice. (A) The diagram illustrating in the process of the research. (B) The body weight of mice. (C) The turning time on the ball of the pole test. (D) The climbing down time from the pole of the pole test. (E) Fall of frequencies of the rotarod test. (F) The time of the first fall of the rotarod test. (G) Total distance traveled in the open filed test. (H) Duration in the center of the open field test. (I) Number of entries travelled in the center of the open field test. (J) Entries explored in the closed arm of the elevated plus maze. (K) Time spent in the closed arm of the elevated plus maze. (L) Entries explored in the open arm of the elevated plus maze. (M) Time spent in the open arm of the elevated plus maze. (N) Time spent in the new arm of the Y maze test. (O) Number of entries in the new arm of the Y maze test. (P) Novel object exploring time and (Q) Total exploration frequencies of the novel object recognition at short term (2 h). (R) Novel object exploring time and (S) Total exploration frequencies of the novel object recognition at long term (24 h). The exploration

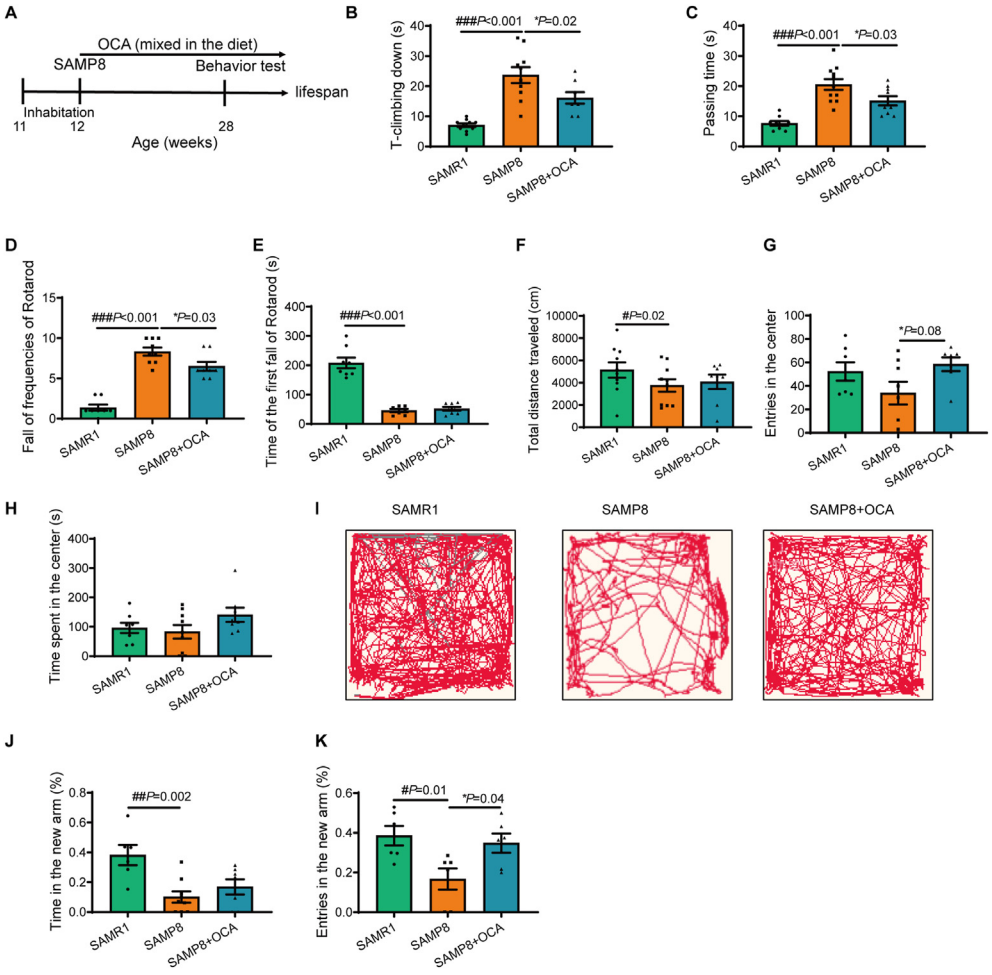

Figure 9 OCA improves healthspan in SAMP8 mice. (A) The OCA treatment diagram of SAMP8 mice. (B) The climbing down time from the pole in the pole test. (C) The passing time spent on the balance beam. (D) The frequencies of fall from the rotarod test. (E) The time of the first fall of the rotarod test. (F) The total distance traveled in the open filed test. (G) The number of entries travelled in the center of the open field test. (H) The duration in the center of the open field test. (I) The track of mice exploring in the open field test. (J) The time spent in the new arm of Y maze test. (K) The number of entries in the new arm of Y maze test. $n \geq 6$ in each group. Data are expressed as mean ± SEM and analyzed by one-way ANOVA. Compared with SAMR1, $^{\#}P < 0.05$, $^{\#\#}P < 0.01$, $^{\#\#\#}P < 0.001$; Compared with SAMP8, $^{*}P < 0.05$, $^{**}P < 0.01$, $^{***}P < 0.001$. SAMR1, Senescence-Accelerated Mouse Resistant 1; SAMP8, Senescence Accelerated Mouse Prone 8. OCA, obeticholic acid.

results showed that the exploring time and frequencies in the new arm of SAMP8 mice were decreased, while OCA treatment increased the entries in the new arm (Fig. 9J and K). Collectively, the results suggest that OCA treatment could reduce motor dysfunction and cognition impairment in SAMP8 mice.

3.11. OCA upregulates detoxifying gene expression via endogenous ligands of PXR

The mechanism of how FXR regulates detoxification gene expression remains largely unclear. It has been reported that FXR may regulate the expression of detoxification genes such as *Abcb1a*, *Fmo3*, and *Gsta2* directly in mice[24]. However, FXR may indirectly regulate the mRNA levels of detoxification genes. Metabolomics plays important roles in pharmacological research, including discovering biomarkers for diseases and explaining the mechanism of action of drugs[98]. Therefore, we analyzed metabolite profiles of the liver of D-gal treated mice to explore whether OCA could increase the internal Pxr and Car transactivity as well as the influence on aging using LC−MS and GC−MS. In LC−MS assay, unsupervised principal component analysis (PCA) showed the distribution of the samples among the control, model, and

time = the novel object exploration time/the old object exploration time. The exploration frequencies = the novel object exploration frequencies/the old object exploration frequencies ($n = 10$ in each group). (T) H&E staining of the CA3 area of the hippocampus. Scale bar, 100 μm. (U) The quantification of damaged neurons in the CA3 area. (V) TUNEL staining of the CA3 area. Scale bar, 100 μm. (W) Apoptosis in the CA3 area. Data are expressed as mean ± SEM and analyzed by one-way ANOVA. Compared with ctrl group, $^{\#}P < 0.05$, $^{\#\#}P < 0.01$, $^{\#\#\#}P < 0.001$; Compared with D-gal group, $^{*}P < 0.05$, $^{**}P < 0.01$, $^{***}P < 0.001$. D-gal, D-galactose; OCA, obeticholic acid.

OCA group (Fig. 10A). And in a supervised OPLS-DA, there was good separation between the OCA and model group, indicating that metabolic perturbation had occurred in OCA and model group (Fig. 10B). Volcano plots were used to determine the difference in metabolites between the model and OCA group. Based on VIP >1, FC >1 and $P<0.05$ values, 62 metabolites were upregulated, and 90 metabolites were downregulated in the liver of OCA-treated mice analyzed by LC−MS (Fig. 10C). KEGG clarified the metabolic pathways upregulated after OCA treatment, including pantothenate and CoA biosynthesis, β-alanine metabolism, glycine, serine, and threonine metabolism, fatty acid degradation, glycerophospholipid metabolism, pyrimidine metabolism (Fig. 10D). Pantothenate, as a vitamin, is required to sustain life, and it is needed to form CoA and is critical in the metabolism and synthesis of protein, fat, and carbohydrates, it had been reported that pantothenate acid is a lifespan-extending agent, and it might have anti-aging effect by itself or by synthesizing other vitamins[99]. Meanwhile, the pyrimidine metabolism pathway is identified to be associated with aging regulation, and supplementation of pyrimidine intermediates could extend the lifespan of nematodes[100,101]. β-Alanine metabolism and glycerophospholipid metabolism also played important roles in the aging process, which involved in tricarboxylic acid cycle (TCA cycle) participating in several aging-regulating mechanisms[102]. Glycine, serine, and threonine metabolism were significantly enriched in aged males receiving young feces transplantation[103]. Fatty acid degradation is responsible for energy production, and its products are also involved in the TCA cycle, which subsequently benefits lifespan-extending. In the GC−MS assay, there were significant differences among the OCA, model, and control group, as shown in PCA (Supporting Information Fig. S7A), indicating the liver metabolic profiles of the three groups were significantly different. The OPLS-DA showed the potential differential metabolites between OCA and the model group (Fig. S7B). Volcano plot analyzed by GC−MS indicated that 9 metabolites were upregulated, and 53 metabolites were downregulated (Fig. 10E). Metabolic pathway enrichment analysis of differential metabolites based on the KEGG database showed that the top 20 pathways were butanoate metabolism, GABAergic synapse, cAMP signaling pathway, alanine, aspartate and glutamate metabolism, synthesis and degradation of ketone bodies, estrogen signaling pathway, GnRH secretion, D-glutamine and D-glutamate metabolism, HIF-1 signaling pathway, oxidative phosphorylation and citrate cycle, etc (Fig. 10F), which were correlated with lipid metabolism and aging regulation effects[104]. Taken together, the metabolomics data indicate that OCA could reverse the metabolism disorder, and the differential metabolites may be mediators of lifespan extension.

Next, we analyzed the differentiated metabolites between D-gal and OCA group and found that (*R*)-3-hydroxybutyric acid, glycerol monostearate, and palmitoylglycine were increased in the liver of OCA-treated mice (Fig. 10G−I). (*R*)-3-Hydroxybutyric acid, an important energy homeostasis indicator, is used as an antioxidant and anti-aging marker in *C. elegans*[105,106]. It is well known that nuclear receptors PXR and CAR are responses to regulate the expression of detoxification genes, such as *CYPs*, *GSTs*, and *ABC Transporters*[107]. Recently, we have revealed that targeting PXR may extend lifespan and healthspan in *C. elegans* and mice through the activation of detoxification functions[71]. To explore the mechanisms of the detoxification effects of OCA, we analyzed the metabolites using a reporter gene assay to explore whether they could activate PXR or CAR transactivity. The results show that palmitoylglycine and *R*-3-hydroxybutyric acid, activated PXR transactivity (Fig. S7C−S7E), while glycerol monostearate and palmitoylglycine activated CAR transactivity (Fig. S7F−S7H), indicating that the compounds may be an endogenous agonist of PXR/CAR. Finally, we assayed the lifespan extension effects of glycerol monostearate and *R*-3-hydroxybutyric acid. The results showed that all the compounds could prolong the lifespan versus vehicle control (Fig. 10J and K and Supporting Information Table S8). Our results indicate that the longevity effects of OCA may be through the activation of PXR or CAR-mediated detoxification function by the endogenous compounds.

4. Discussion

FXR is a ligand-activated nuclear receptor transcription factor with many biological functions, including lipid and glucose homeostasis regulation, bile acid, and steroid metabolism *via* its downstream genes. Here we show that FXR agonist OCA not only extended lifespan in *C elegans*, but also improved motor ability, cardiac fibrosis, inflammation, learning, and memory impairment in drug-induced early senescent mice.

OCA is a marked drug for cholestasis and a potential drug for non-alcoholic fatty liver disease[108]. We showed that OCA extended the survival rates of worms at multiple concentrations. In a previous study, Morshead et al. concluded that OCA could not extend lifespan in nematodes at a dose of 50, 100, and 150 μmol/L by using flatbed scanner-based Automated Lifespan Machine workflow[55], which lacks physiological relevance of OCA to *C. elegans*. The discrepancy between the two studies is probably caused by several reasons. First, the upregulation of FXR can lead to a negative feedback mechanism reducing FXR levels[109]. Second, high concentrations of OCA might cause off-target effects, which impair the longevity effect of OCA. Finally, the starting point of lifespan experiments was different, which was started on day one of adulthood in the previous study, and the L4 stage in this study. In the present study, we also assayed several other FXR agonists on the survival rate of worms. The data revealed that FXR agonists showed similar lifespan-extending effects on *C. elegans*. To confirm that OCA extends lifespan through nuclear receptors, we analyzed the effects of OCA on *nhr-8* and *daf-12* mutant worms. The longevity effects of OCA were attenuated in these mutant worms, further supporting that FXR may serve as a longevity target.

Recently, we have reported that targeting PXR-mediated detoxification function may extend lifespan and healthspan in animals[71]. FXR and PXR also regulate bile acid synthesis and circulation, while bile acids are endogenous FXR and PXR ligands. In *C. elegans*, bile acid-like steroids dafachronic acids regulate development and longevity through DAF-12[34]. OCA is a well-studied synthetic bile acid and potent FXR agonist in clinical trials for liver fibrosis[23]. In the present study, we demonstrated that OCA may increase the resistance of worms and mice to xenobiotics, similar to PXR agonists. When worms were exposed to MeHgCl, PQ, CC, and CQ, the survival rate of worms was significantly reduced, while OCA counteracted the toxic effects of these xenobiotics in a dose-dependent manner. Furthermore, L02 cells were exposed to PQ, MeHgCl, CC, and CQ, and we found that OCA increased L02 cell viability exposed to PQ, CC, and CQ. These data indicated that OCA upregulated detoxification effects both *in vivo* and *in vitro*. Meanwhile, OCA upregulated the gene expression of detoxifying enzymes, such as *Cyps*, *Gsts*, and *Abc transporters*, in both worms and mice. These results were supported by the RNA sequence analysis using the liver of the mice,

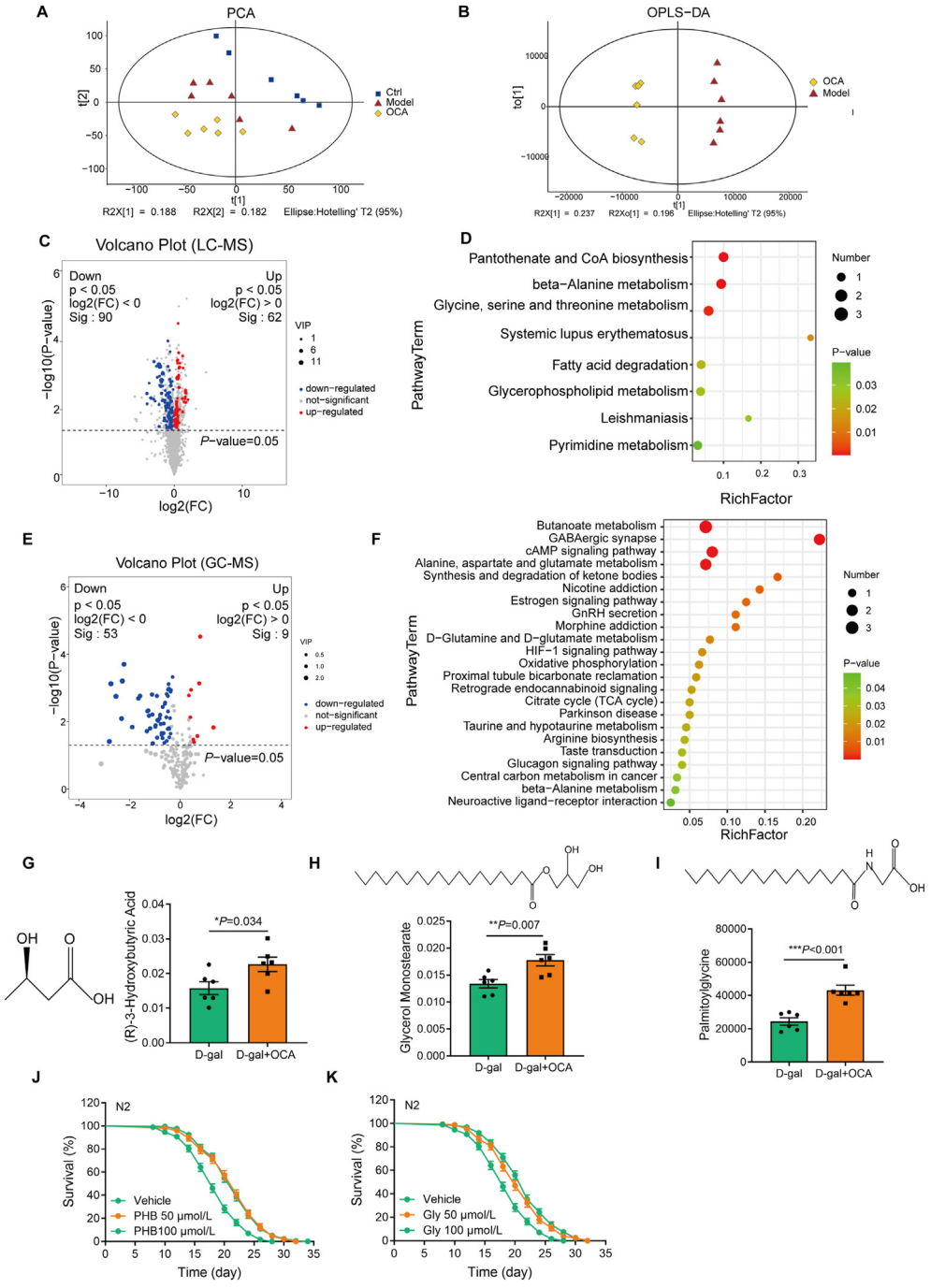

Figure 10 OCA increases detoxifying gene expression *via* the internal ligands of PXR. (A) Plots of principal component analysis (PCA) among control, D-gal and OCA group. (B) Orthogonal PLS-DA (OPLS-DA). The *x*- and *y*-axes represent the first (PCA1) and second (PC2)/orthogonal (PCo1) principal components, respectively. (C) Volcano plot analysis of the differentially expressed metabolites (DEMs) in LC−MS. The red/blue dots in the figure represent up/downregulated DEMs, and the gray dots represent metabolite that no changed. (D) Upregulated pathway in the Kyoto Encyclopedia of Genes and Genomes (KEGG) analysis of DEMs in LC−MS. The *x*- and *y*-axes indicate the enrichment factor and pathway term, respectively. The colors and sizes of dots represent the significance and number of metabolites. There are three samples in each group. (E) Volcano plot analysis of the differentially expressed metabolites (DEMs) in GC−MS. The red/blue dots in the figure represent up/downregulated DEMs, and the gray dots represent metabolite that no changed. (F) Upregulated pathway in the Kyoto Encyclopedia of Genes and Genomes (KEGG) analysis of DEMs in GC−MS. (G) (*R*)-3-Hydroxybutyric acid content. (H) Glycerol monostearate content. (I) Palmitoylglycine content ($n = 3$). Survival curve of N2 worms treated with (*R*)-3-hydroxybutyric acid (J); Glycerol monostearate (K). The lifespan of worms was performed at 20 °C, and analyzed by log-rank test. The detailed lifespan analysis is listed in Table S8. Significance was analyzed by (G−J) two-tailed unpaired Student's *t*-test. Data are expressed as mean ± SEM. Compared with control group, $^{\#}P < 0.05$, $^{\#\#}P < 0.01$ $^{\#\#\#}P < 0.001$; Compared with D-gal group, $^{*}P < 0.05$, $^{**}P < 0.01$, $^{***}P < 0.001$. PHB, (*R*)-3-hydroxybutyric acid. Gly, glycerol monostearate. OCA, obeticholic acid.

which also showed that the expression of detoxification genes was increased. Interestingly, the transcription characteristics of OCA mice are similar to that of 17 other longevity interventions, which Tyshkovskiy reported[20]. The detoxifying effect of OCA on lifespan extension and healthspan improvement in *C. elegans* and mice may provide new insights into the mechanisms underlying aging.

One of the major functions of FXR is regulating lipid and glucose homeostasis. We performed the lifespan experiment using the orthologue of IGFR pathway molecules, *daf-2* and *daf-16* mutants and illuminated that the lifespan of *daf-2* and *daf-16* mutants was not extended by OCA. The lipid metabolism pathways in mammals, including fatty acid synthesis, elongation and desaturation, glycolysis, gluconeogenesis, amino acid metabolism, and mitochondrial and peroxisomal β-oxidation of fatty acids[110] are well conserved in *C. elegans*. In *C. elegans*, fat metabolism is an important factor involved in longevity. The rate-limiting enzymes in the conversion of MUFAs to PUFAs, fat-5, fat-6, and fat-7 were blocked, and the lifespan expansion effect was diminished, indicating that OCA was involved in PUFAs synthesis. Meanwhile, when fat-2 and fat-3 were blocked, the lifespan extension effect was also diminished. These data all indicated that OCA treatment increased lifespan was related to lipid metabolism. Moreover, AMPK and mTOR, as two important hubs in sensing nutrition, OCA's extended lifespan may also be associated with those two key regulators. As an energy store, mitochondria are important for energy homeostasis, OCA treatment enhanced mitochondrial content in old worms. These data indicated that OCA regulated lipid metabolism and energy metabolism in nematodes, subsequently extending the lifespan and improving organelles' fitness. These results suggest that the longevity effects of OCA may be relevant to the regulation of glucose and lipids.

In D-gal and Dox-induced early senescent mice, OCA treatment also significantly enhanced motor ability and extended the survival time. Through behavioral tests, we found that OCA treatment not only enhanced the mobility defects but also improved the cognition impairment. At the same time, OCA alleviated the neurons' degenerative and cell inflammatory infiltration in the liver and the heart and reduced apoptosis in the CA3 region of the hippocampus. In Dox-induced early senescent mice, OCA significantly increased the lifespan and improved liver inflammation and motor defects. Notably, OCA treatment inhibited the biomarkers of pre-aging factors, including *p53*, *p21*, and *p16*, and SASP inflammatory cytokines *Il-6*, *Il1b*, and *Tnfa*, which was consistent with the previous reports showing that FXR may inhibit NF-kB mediated inflammation[111]. Taken together, these data indicated that OCA could counteract chemical drug-induced aging in mice and improve body function.

As a potent FXR agonist, OCA selectively activates FXR to upregulate the expression of some detoxifying genes[24]. However, in the present study, many detoxification genes, including phase I *Cyps*, phase II *Gsts*, and *Abc transporters*, were transcriptionally regulated by OCA with RAN-Seq and qRT-PCR analysis. How did OCA regulate a spectrum of detoxification machinery? Untargeted metabolites of D-gal-induced aging mice indicated that the metabolites enriched in the OCA treatment group increased PXR and CAR transactivity. Notably, a previous study reported that PXR is the downstream target of FXR[112]. At the transcriptional and protein levels, OCA treatment activated the genes and proteins downstream of PXR. Interestingly, the enhanced metabolites in OCA-treated mice could extend the lifespan of N2 worms. These data all indicate that OCA, as an agonist of FXR, may activate detoxification gene expression through multiple mechanisms. Furthermore, OCA treatment also improved motor ability dysfunction and cognition impairment in SAMP8 mice, which indicates that although OCA can cause side effects in clinics, a lower dosage of OCA may improve the healthspan not only in chemical-induced aging mice but also in genetically accelerated senescent mice.

Our studies have demonstrated that OCA may extend lifespan in *C. elegans* and Dox-induced early senescent mice, enhance the capacity of toxic resistance, alleviate inflammation, and improve learning and memory as well as neuroprotective effect in mice. The underlying mechanism is probably due to the activation of detoxifying gene expression, subsequently increasing xenobiotics metabolism. Our results suggest that FXR is a potential longevity drug target.

5. Conclusions

Our findings revealed that OCA, as a classic FXR agonist, has the potential to lengthen lifespan and improve healthspan by activating nuclear receptors-mediated detoxification functions in *C. elegans* and the liver of mice. Thus, targeting liver FXR may promote longevity.

Acknowledgements

This work was supported by the National Natural Science Foundation of China (82073951) to Cheng Huang and the Fok Ying Tung Education Foundation (171036) to Shengjie Fan.

Author contributions

Lijun Zhang: Writing − original draft, Validation, Software, Methodology, Investigation, Data curation. Jing Yu: Methodology, Data curation. Xiaoyan Gao: Methodology, Formal analysis, Data curation. Yingxuan Yan: Methodology, Investigation, Data curation. Xinyi Wang: Methodology, Investigation, Data curation. Hang Shi: Methodology, Investigation. Minglv Fang: Methodology, Investigation. Ying Liu: Methodology, Investigation. Young-Bum Kim: Writing − review & editing, Visualization, Project administration, Conceptualization. Huanhu Zhu: Writing − review & editing, Visualization, Supervision, Project administration, Conceptualization. Xiaojun Wu: Writing − review & editing, Visualization, Project administration, Conceptualization. Cheng Huang: Writing − review & editing, Supervision, Project administration, Methodology, Funding acquisition, Conceptualization. Shengjie Fan: Writing − review & editing, Visualization, Supervision, Project administration, Methodology, Funding acquisition, Conceptualization.

Conflicts of interest

The authors declare no conflicts of interest.

Appendix A. Supporting information

Supporting information to this article can be found online at https://doi.org/10.1016/j.apsb.2025.01.006.

References

1. Hahad O, Frenis K, Kuntic M, Daiber A, Münzel T. Accelerated aging and age-related diseases (CVD and neurological) due to air pollution and traffic noise exposure. *Int J Mol Sci* 2021;**22**:2419.
2. Rackova L, Mach M, Brnoliakova Z. An update in toxicology of ageing. *Environ Toxicol Pharmacol* 2021;**84**:103611.
3. Pearson BL, Ehninger D. Environmental chemicals and aging. *Curr Environ Health Rep* 2017;**4**:38−43.
4. Gao X, Coull B, Lin X, Vokonas P, Spiro 3rd A, Hou L, et al. Short-term air pollution, cognitive performance, and nonsteroidal anti-inflammatory drug use in the Veterans Affairs Normative Aging Study. *Nat Aging* 2021;**1**:430−7.
5. Murphy CT, Hu PJ. Insulin/insulin-like growth factor signaling in *C. elegans*. *WormBook* 2013:1−43.
6. Cohen E, Paulsson JF, Blinder P, Burstyn-Cohen T, Du D, Estepa G, et al. Reduced IGF-1 signaling delays age-associated proteotoxicity in mice. *Cell* 2009;**139**:1157−69.
7. Honda Y, Honda S. The *daf-2* gene network for longevity regulates oxidative stress resistance and Mn-superoxide dismutase gene expression in *Caenorhabditis elegans*. *FASEB J* 1999;**13**:1385−93.
8. Riedel CG, Dowen RH, Lourenco GF, Kirienko NV, Heimbucher T, West JA, et al. DAF-16 employs the chromatin remodeller SWI/SNF to promote stress resistance and longevity. *Nat Cell Biol* 2013;**15**:491−501.
9. Kwon ES, Narasimhan SD, Yen K, Tissenbaum HA. A new DAF-16 isoform regulates longevity. *Nature* 2010;**466**:498−502.
10. Slack C, Giannakou ME, Foley A, Goss M, Partridge L. dFOXO-independent effects of reduced insulin-like signaling in *Drosophila*. *Aging Cell* 2011;**10**:735−48.
11. Aidoo A, Desai VG, Lyn-Cook LE, Chen JJ, Feuers RJ, Casciano DA. Attenuation of bleomycin-induced Hprt mutant frequency in female and male rats by calorie restriction. *Mutat Res* 1999;**430**:155−63.
12. Apte UM, Limaye PB, Desaiah D, Bucci TJ, Warbritton A, Mehendale HM. Mechanisms of increased liver tissue repair and survival in diet-restricted rats treated with equitoxic doses of thioacetamide. *Toxicol Sci* 2003;**72**:272−82.
13. Harper JM, Salmon AB, Chang Y, Bonkowski M, Bartke A, Miller RA. Stress resistance and aging: influence of genes and nutrition. *Mech Ageing Dev* 2006;**127**:687−94.
14. Miller RA, Buehner G, Chang Y, Harper JM, Sigler R, Smith-Wheelock M. Methionine-deficient diet extends mouse lifespan, slows immune and lens aging, alters glucose, T4, IGF-I and insulin levels, and increases hepatocyte MIF levels and stress resistance. *Aging Cell* 2005;**4**:119−25.
15. Hoffmann JM, Partridge L. Nuclear hormone receptors: roles of xenobiotic detoxification and sterol homeostasis in healthy aging. *Crit Rev Biochem Mol Biol* 2015;**50**:380−92.
16. Amador-Noguez D, Dean A, Huang W, Setchell K, Moore D, Darlington G. Alterations in xenobiotic metabolism in the long-lived little mice. *Aging Cell* 2007;**6**:453−70.
17. Amador-Noguez D, Yagi K, Venable S, Darlington G. Gene expression profile of long-lived Ames dwarf mice and little mice. *Aging Cell* 2004;**3**:423−41.
18. Miller RA, Harrison DE, Astle CM, Fernandez E, Flurkey K, Han M, et al. Rapamycin-mediated lifespan increase in mice is dose and sex dependent and metabolically distinct from dietary restriction. *Aging Cell* 2014;**13**:468−77.
19. Steinbaugh MJ, Sun LY, Bartke A, Miller RA. Activation of genes involved in xenobiotic metabolism is a shared signature of mouse models with extended lifespan. *Am J Physiol Endocrinol Metab* 2012;**303**:E488−95.
20. Tyshkovskiy A, Bozaykut P, Borodinova AA, Gerashchenko MV, Ables GP, Garratt M, et al. Identification and application of gene expression signatures associated with lifespan extension. *Cell Metab* 2019;**30**:573−593.e8.
21. Hunt NJ, Kang SWS, Lockwood GP, Le Couteur DG, Cogger VC. Hallmarks of aging in the liver. *Comput Struct Biotechnol J* 2019;**17**:1151−61.
22. Samur S, Klebanoff M, Banken R, Pratt DS, Chapman R, Ollendorf DA, et al. Long-term clinical impact and cost-effectiveness of obeticholic acid for the treatment of primary biliary cholangitis. *Hepatology* 2017;**65**:920−8.
23. Younossi ZM, Ratziu V, Loomba R, Rinella M, Anstee QM, Goodman Z, et al. Obeticholic acid for the treatment of non-alcoholic steatohepatitis: interim analysis from a multicentre, randomised, placebo-controlled phase 3 trial. *Lancet* 2019;**394**:2184−96.
24. Jiang Y, Jin J, Iakova P, Hernandez JC, Jawanmardi N, Sullivan E, et al. Farnesoid X receptor directly regulates xenobiotic detoxification genes in the long-lived Little mice. *Mech Ageing Dev* 2013;**134**:407−15.
25. Peng L, Piekos S, Guo GL, Zhong XB. Role of farnesoid X receptor in establishment of ontogeny of phase-I drug metabolizing enzyme genes in mouse liver. *Acta Pharm Sin B* 2016;**6**:453−9.
26. Wang XX, Luo Y, Wang D, Adorini L, Pruzanski M, Dobrinskikh E, et al. A dual agonist of farnesoid X receptor (FXR) and the G protein-coupled receptor TGR5, INT-767, reverses age-related kidney disease in mice. *J Biol Chem* 2017;**292**:12018−24.
27. Li Z, Huang J, Wang F, Li W, Wu X, Zhao C, et al. Dual targeting of bile acid receptor-1 (TGR5) and farnesoid X receptor (FXR) prevents estrogen-dependent bone loss in mice. *J Bone Miner Res* 2019;**34**:765−76.
28. Xiong X, Wang X, Lu Y, Wang E, Zhang Z, Yang J, et al. Hepatic steatosis exacerbated by endoplasmic reticulum stress-mediated downregulation of FXR in aging mice. *J Hepatol* 2014;**60**:847−54.
29. Bjursell M, Wedin M, Admyre T, Hermansson M, Böttcher G, Göransson M, et al. Ageing Fxr deficient mice develop increased energy expenditure, improved glucose control and liver damage resembling NASH. *PLoS One* 2013;**8**:e64721.
30. Qiu Y, Yu J, Ji X, Yu H, Xue M, Zhang F, et al. Ileal FXR-FGF15/19 signaling activation improves skeletal muscle loss in aged mice. *Mech Ageing Dev* 2022;**202**:111630.
31. Chamoli M, Singh A, Malik Y, Mukhopadhyay A. A novel kinase regulates dietary restriction-mediated longevity in *Caenorhabditis elegans*. *Aging Cell* 2014;**13**:641−55.
32. Thondamal M, Witting M, Schmitt-Kopplin P, Aguilaniu H. Steroid hormone signalling links reproduction to lifespan in dietary-restricted *Caenorhabditis elegans*. *Nat Commun* 2014;**5**:4879.
33. Hsin H, Kenyon C. Signals from the reproductive system regulate the lifespan of *C. elegans*. *Nature* 1999;**399**:362−6.
34. Wollam J, Magner DB, Magomedova L, Rass E, Shen Y, Rottiers V, et al. A novel 3-hydroxysteroid dehydrogenase that regulates reproductive development and longevity. *Plos Biol* 2012;**10**:e1001305.
35. Mahanti P, Bose N, Bethke A, Judkins JC, Wollam J, Dumas KJ, et al. Comparative metabolomics reveals endogenous ligands of DAF-12, a nuclear hormone receptor, regulating *C. elegans* development and lifespan. *Cell Metab* 2014;**19**:73−83.
36. Fisher AL, Lithgow GJ. The nuclear hormone receptor DAF-12 has opposing effects on *Caenorhabditis elegans* lifespan and regulates genes repressed in multiple long-lived worms. *Aging Cell* 2006;**5**:127−38.
37. Brenner S. The genetics of *Caenorhabditis elegans*. *Genetics* 1974;**77**:71−94.
38. Porta-de-la-Riva M, Fontrodona L, Villanueva A, Ceron J. Basic *Caenorhabditis elegans* methods: synchronization and observation. *J Vis Exp* 2012;**64**:e4019.
39. Chen Y, Onken B, Chen H, Xiao S, Liu X, Driscoll M, et al. Mechanism of longevity extension of *Caenorhabditis elegans* induced by pentagalloyl glucose isolated from eucalyptus leaves. *J Agric Food Chem* 2014;**62**:3422−31.
40. Tsalik EL, Hobert O. Functional mapping of neurons that control locomotory behavior in *Caenorhabditis elegans*. *J Neurobiol* 2003;**56**:178−97.

41. Liu Y, Zhou Z, Yin L, Zhu M, Wang F, Zhang L, et al. Tangeretin promotes lifespan associated with insulin/insulin-like growth factor-1 signaling pathway and heat resistance in *Caenorhabditis elegans*. *Biofactors* 2022;**48**:442−53.
42. Kechin A, Boyarskikh U, Kel A, Filipenko M. CutPrimers: a new tool for accurate cutting of primers from reads of targeted next generation sequencing. *J Comput Biol* 2017;**24**:1138−43.
43. Kim D, Langmead B, Salzberg SL. HISAT: a fast spliced aligner with low memory requirements. *Nat Methods* 2015;**12**:357−60.
44. Pertea M, Pertea GM, Antonescu CM, Chang TC, Mendell JT, Salzberg SL. StringTie enables improved reconstruction of a transcriptome from RNA-seq reads. *Nat Biotechnol* 2015;**33**:290−5.
45. Love MI, Huber W, Anders S. Moderated estimation of fold change and dispersion for RNA-seq data with DESeq2. *Genome Biol* 2014;**15**:550.
46. Wu T, Hu E, Xu S, Chen M, Guo P, Dai Z, et al. clusterProfiler 4.0: a universal enrichment tool for interpreting omics data. *Innov* 2021;**2**:100141.
47. Kamath RS, Martinez-Campos M, Zipperlen P, Fraser AG, Ahringer J. Effectiveness of specific RNA-mediated interference through ingested double-stranded RNA in *Caenorhabditis elegans*. *Genome Biol* 2001;**2**:Research0002.
48. Carter RJ, Morton J, Dunnett SB. Motor coordination and balance in rodents. *Curr Protoc Neurosci* 2001;**15**. Chapter 8:Unit 8.12.
49. Lu J, Zheng YL, Wu DM, Luo L, Sun DX, Shan Q. Ursolic acid ameliorates cognition deficits and attenuates oxidative damage in the brain of senescent mice induced by D-galactose. *Biochem Pharmacol* 2007;**74**:1078−90.
50. Komada M, Takao K, Miyakawa T. Elevated plus maze for mice. *J Vis Exp* 2008;**22**:1088.
51. Kraeuter AK, Guest PC, Sarnyai Z. The Y-Maze for assessment of spatial working and reference memory in mice. *Methods Mol Biol* 2019;**1916**:105−11.
52. Lueptow LM. Novel object recognition test for the investigation of learning and memory in mice. *J Vis Exp* 2017;**126**:55718.
53. Huang C, Zhang Y, Gong Z, Sheng X, Li Z, Zhang W, et al. Berberine inhibits 3T3-L1 adipocyte differentiation through the PPARgamma pathway. *Biochem Biophys Res Commun* 2006;**348**:571−8.
54. Shen P, Yue Y, Sun Q, Kasireddy N, Kim KH, Park Y. Piceatannol extends the lifespan of *Caenorhabditis elegans via* DAF-16. *Biofactors* 2017;**43**:379−87.
55. Morshead ML, Sedore CA, Jones EG, Hall D, Plummer WT, Garrett T, et al. Caenorhabditis Intervention Testing Program: the farnesoid X receptor agonist obeticholic acid does not robustly extend lifespan in nematodes. *Micropubl Biol* 2020;**2020**:10.17912/micropub.biology.000257.
56. Melzer D, Pilling LC, Ferrucci L. The genetics of human ageing. *Nat Rev Genet* 2020;**21**:88−101.
57. Cabreiro F, Au C, Leung KY, Vergara-Irigaray N, Cochemé HM, Noori T, et al. Metformin retards aging in *C. elegans* by altering microbial folate and methionine metabolism. *Cell* 2013;**153**:228−39.
58. Wainer-Katsir K, Zou JY, Linial M. Extended fertility and longevity: the genetic and epigenetic link. *Fertil Steril* 2015;**103**:1117−24.
59. Broughton S, Partridge L. Insulin/IGF-like signalling, the central nervous system and aging. *Biochem J* 2009;**418**:1−12.
60. Fontana L, Partridge L, Longo VD. Extending healthy life span—-from yeast to humans. *Science* 2010;**328**:321−6.
61. Friedman DB, Johnson TE. A mutation in the age-1 gene in *Caenorhabditis elegans* lengthens life and reduces hermaphrodite fertility. *Genetics* 1988;**118**:75−86.
62. Ewald CY, Hourihan JM, Bland MS, Obieglo C, Katic I, Moronetti Mazzeo LE, et al. NADPH oxidase-mediated redox signaling promotes oxidative stress resistance and longevity through memo-1 in *C. elegans*. *Elife* 2017;**6**:e19493.
63. Kumsta C, Chang JT, Schmalz J, Hansen M. Hormetic heat stress and HSF-1 induce autophagy to improve survival and proteostasis in *C. elegans*. *Nat Commun* 2017;**8**:14337.
64. Wei P, Zhang J, Egan-Hafley M, Liang S, Moore DD. The nuclear receptor CAR mediates specific xenobiotic induction of drug metabolism. *Nature* 2000;**407**:920−3.
65. Czuba LC, Hillgren KM, Swaan PW. Post-translational modifications of transporters. *Pharmacol Ther* 2018;**192**:88−99.
66. Brinkmann V, Ale-Agha N, Haendeler J, Ventura N. The aryl hydrocarbon receptor (AhR) in the aging process: another puzzling role for this highly conserved transcription factor. *Front Physiol* 2019;**10**:1561.
67. Blackwell TK, Steinbaugh MJ, Hourihan JM, Ewald CY, Isik M. SKN-1/Nrf, stress responses, and aging in *Caenorhabditis elegans*. *Free Radic Biol Med* 2015;**88**:290−301.
68. Lindblom TH, Dodd AK. Xenobiotic detoxification in the nematode *Caenorhabditis elegans*. *J Exp Zool Comp Exp Biol* 2006;**305**:720−30.
69. Mackowiak B, Wang H. Mechanisms of xenobiotic receptor activation: direct *vs*. indirect. *Biochim Biophys Acta* 2016;**1859**:1130−40.
70. Oladimeji PO, Chen T. PXR: more than just a master xenobiotic receptor. *Mol Pharmacol* 2018;**93**:119−27.
71. Fan S, Yan Y, Xia Y, Zhou Z, Luo L, Zhu M, et al. Pregnane X receptor agonist nomilin extends lifespan and healthspan in preclinical models through detoxification functions. *Nat Commun* 2023;**14**:3368.
72. Robida-Stubbs S, Glover-Cutter K, Lamming Dudley W, Mizunuma M, Narasimhan Sri D, Neumann-Haefelin E, et al. TOR signaling and rapamycin influence longevity by regulating SKN-1/Nrf and DAF-16/FoxO. *Cell Metab* 2012;**15**:713−24.
73. Kalaany NY, Mangelsdorf DJ. LXRS and FXR: the yin and yang of cholesterol and fat metabolism. *Annu Rev Physiol* 2006;**68**:159−91.
74. González A, Hall MN, Lin SC, Hardie DG. AMPK and TOR: the Yin and Yang of cellular nutrient sensing and growth control. *Cell Metab* 2020;**31**:472−92.
75. Chen J, Ou Y, Li Y, Hu S, Shao LW, Liu Y. Metformin extends *C. elegans* lifespan through lysosomal pathway. *Elife* 2017;**6**:e31268.
76. Li W, Chen S, Lang J, Luo J, Chen J, Zhang L, et al. The clinical antiprotozoal drug nitazoxanide and its metabolite tizoxanide extend *Caenorhabditis elegans* lifespan and healthspan. *Acta Pharm Sin B* 2024;**14**:3266−80.
77. Lakowski B, Hekimi S. The genetics of caloric restriction in *Caenorhabditis elegans*. *Proc Natl Acad Sci U S A* 1998;**95**:13091−6.
78. Hashimoto Y, Ookuma S, Nishida E. Lifespan extension by suppression of autophagy genes in *Caenorhabditis elegans*. *Genes Cells* 2009;**14**:717−26.
79. Wang Y, Hekimi S. Mitochondrial dysfunction and longevity in animals: untangling the knot. *Science* 2015;**350**:1204−7.
80. Hernandez-Segura A, Nehme J, Demaria M. Hallmarks of cellular senescence. *Trends Cell Biol* 2018;**28**:436−53.
81. Guo Y, Guan T, Shafiq K, Yu Q, Jiao X, Na D, et al. Mitochondrial dysfunction in aging. *Ageing Res Rev* 2023;**88**:101955.
82. Mao Z, Liu W, Huang Y, Sun T, Bao K, Feng J, et al. Anti-aging effects of chlorpropamide depend on mitochondrial complex-II and the production of mitochondrial reactive oxygen species. *Acta Pharm Sin B* 2022;**12**:665−77.
83. Rowland A, Miners JO, Mackenzie PI. The UDP-glucuronosyltransferases: their role in drug metabolism and detoxification. *Int J Biochem Cell Biol* 2013;**45**:1121−32.
84. Sun T, Zhang L, Feng J, Bao L, Wang J, Song Z, et al. Characterization of cellular senescence in doxorubicin-induced aging mice. *Exp Gerontol* 2022;**163**:111800.
85. Baar MP, Brandt RMC, Putavet DA, Klein JDD, Derks KWJ, Bourgeois BRM, et al. Targeted apoptosis of senescent cells restores tissue homeostasis in response to chemotoxicity and aging. *Cell* 2017;**169**:132−47.e16.
86. Chávez-Talavera O, Tailleux A, Lefebvre P, Staels B. Bile acid control of metabolism and inflammation in obesity, type 2 diabetes, dyslipidemia, and nonalcoholic fatty liver disease. *Gastroenterology* 2017;**152**:1679−94.e3.
87. Xu Y, Wu T, Jin Y, Fu Z. Effects of age and jet lag on D-galactose induced aging process. *Biogerontology* 2009;**10**:153−61.

88. Ahmad S, Khan A, Ali W, Jo MH, Park J, Ikram M, et al. Fisetin rescues the mice brains against D-galactose-induced oxidative stress, neuroinflammation and memory impairment. *Front Pharmacol* 2021; **12**:612078.
89. Wei H, Li L, Song Q, Ai H, Chu J, Li W. Behavioural study of the D-galactose induced aging model in C57BL/6J mice. *Behav Brain Res* 2005;**157**:245−51.
90. Zhang Y, Roy DS, Zhu Y, Chen Y, Aida T, Hou Y, et al. Targeting thalamic circuits rescues motor and mood deficits in PD mice. *Nature* 2022;**607**:321−9.
91. Prut L, Belzung C. The open field as a paradigm to measure the effects of drugs on anxiety-like behaviors: a review. *Eur J Pharmacol* 2003;**463**:3−33.
92. Yoshizaki K, Asai M, Hara T. High-fat diet enhances working memory in the Y-Maze test in male C57BL/6J mice with less anxiety in the elevated plus maze test. *Nutrients* 2020;**12**:2036.
93. Antunes M, Biala G. The novel object recognition memory: neurobiology, test procedure, and its modifications. *Cogn Process* 2012;**13**: 93−110.
94. Wang LF, Cao Q, Wen K, Xiao YF, Chen TT, Guan XH, et al. CD38 deficiency alleviates D-galactose-induced myocardial cell senescence through NAD^+/Sirt1 signaling pathway. *Front Physiol* 2019;**10**:1125.
95. Takeda T. Senescence-accelerated mouse (SAM) with special references to neurodegeneration models, SAMP8 and SAMP10 mice. *Neurochem Res* 2009;**34**:639−59.
96. Liu B, Liu J, Shi JS. SAMP8 mice as a model of age-related cognition decline with underlying mechanisms in Alzheimer's disease. *J Alzheimers Dis* 2020;**75**:385−95.
97. Yang X, Yu D, Xue L, Li H, Du J. Probiotics modulate the microbiota−gut−brain axis and improve memory deficits in aged SAMP8 mice. *Acta Pharm Sin B* 2020;**10**:475−87.
98. Puchades-Carrasco L, Pineda-Lucena A. Metabolomics in pharmaceutical research and development. *Curr Opin Biotechnol* 2015;**35**:73−7.
99. Kunugi H, Mohammed Ali A. Royal Jelly and its components promote healthy aging and longevity: from animal models to humans. *Int J Mol Sci* 2019;**20**:4662.
100. Wan QL, Meng X, Fu X, Chen B, Yang J, Yang H, et al. Intermediate metabolites of the pyrimidine metabolism pathway extend the lifespan of *C. elegans* through regulating reproductive signals. *Aging (Albany NY)* 2019;**11**:3993−4010.
101. Wan QL, Shi X, Liu J, Ding AJ, Pu YZ, Li Z, et al. Metabolomic signature associated with reproduction-regulated aging in *Caenorhabditis elegans*. *Aging (Albany NY)* 2017;**9**:447−74.
102. Inigo M, Deja S, Burgess SC. Ins and outs of the TCA cycle: the central role of anaplerosis. *Annu Rev Nutr* 2021;**41**:19−47.
103. Tang L, Li J, Sun B, Bai Y, Zhou X, Chen L. Transcriptomic interaction between young fecal transplantation and perfluorobutanesulfonate in aged zebrafish gonads. *Toxics* 2022;**10**:631.
104. Wan H, Liu D, Liu B, Sha M, Xia W, Liu C. Bioinformatics analysis of aging-related genes in thoracic aortic aneurysm and dissection. *Front Cardiovasc Med* 2023;**10**:1089312.
105. Li N, Li Q, He X, Gao X, Wu L, Xiao M, et al. Antioxidant and anti-aging activities of *Laminaria japonica* polysaccharide in *Caenorhabditis elegans* based on metabonomic analysis. *Int J Biol Macromol* 2022;**221**:346−54.
106. Chen Y, Luo Z, Sun Y, Li F, Han Z, Qi B, et al. Exercise improves choroid plexus epithelial cells metabolism to prevent glial cell-associated neurodegeneration. *Front Pharmacol* 2022;**13**:1010785.
107. Negishi M, Kobayashi K, Sakuma T, Sueyoshi T. Nuclear receptor phosphorylation in xenobiotic signal transduction. *J Biol Chem* 2020; **295**:15210−25.
108. Neuschwander-Tetri BA, Loomba R, Sanyal AJ, Lavine JE, Van Natta ML, Abdelmalek MF, et al. Farnesoid X nuclear receptor ligand obeticholic acid for non-cirrhotic, non-alcoholic steatohepatitis (FLINT): a multicentre, randomised, placebo-controlled trial. *Lancet* 2015;**385**:956−65.
109. Fang Y, Hegazy L, Finck BN, Elgendy B. Recent advances in the medicinal chemistry of Farnesoid X receptor. *J Med Chem* 2021;**64**: 17545−71.
110. McKay RM, McKay JP, Avery L, Graff JM. *C. elegans*: a model for exploring the genetics of fat storage. *Dev Cell* 2003;**4**:131−42.
111. Wang YD, Chen WD, Wang M, Yu D, Forman BM, Huang W. Farnesoid X receptor antagonizes nuclear factor kappaB in hepatic inflammatory response. *Hepatology* 2008;**48**:1632−43.
112. Jung D, Mangelsdorf DJ, Meyer UA. Pregnane X receptor is a target of farnesoid X receptor. *J Biol Chem* 2006;**281**:19081−91.